Chem Soc Rev

Cite this: *Chem. Soc. Rev.*, 2012, **41**, 1173–1190

www.rsc.org/csr

CRITICAL REVIEW

Host–guest sensing by calixarenes on the surfaces

Hyun Jung Kim,[a] Min Hee Lee,[a] Lucia Mutihac,*[b] Jacques Vicens*[c] and Jong Seung Kim*[a]

Received 23rd June 2011
DOI: 10.1039/c1cs15169j

The present *critical review* reports on recent developments of optical nanoparticles based on the association of gold, silver, silica and quantum dots and calixarenes. These hybrid organic–inorganic compounds characterized by a thick organic layer self-assembled on the surface of a core of mineral surface atoms take advantage of the supramolecular recognition of luminescent calixarenes to fabricate nanodevices of nanoparticle size, capable of detecting metal cations, polyaromatic hydrocarbons and pesticides. Also presented is an explanation of the involvement of such nanoparticles in biochemical systems. This *critical review* provides an overview of their preparation, the manner in which they are characterized, and their use (108 references).

1. Introduction

Nanotechnology is the construction and use of functional structures designed at molecular scale with at least one characteristic dimension measured in nanometres (10^{-9} m or 10 Å). Their size confers on them the ability to exhibit novel and improved physical, chemical, and biological properties, phenomena, and processes. When characteristic structural features are intermediate—between isolated atoms and bulk materials in the range of about one to 100 nanometres—the objects frequently display physical characteristics different from those evidenced by either atoms or bulk materials.

Events at the nanometre scale are likely to constitute a completely new phenomenology. The properties of matter are not as predictable as those at larger scales. Changes in properties are due not only to the continuous modification of characteristics with diminishing size, but also to the occurrence of new phenomena such as quantum confinement, a typical example of which is that the color of light emitted from semiconductor nanoparticles depends on their sizes.

Nanotechnology can provide us with unprecedented understanding of materials and devices that are useful in a variety of fields. By tuning the structure on the nanoscale, one

[a] *Department of Chemistry, Korea University, Seoul 136-701, South Korea. E-mail: jongskim@korea.ac.kr*
[b] *Department of Analytical Chemistry, University of Bucharest, 4-12 Regina Elisabeta Blvd, 030018 Bucharest, Romania. E-mail: mutihac@astralnet.ro*
[c] *IPHC-UdS-ECPM-CNRS, 25, rue Becquerel, 67087 Strasbourg, France. E-mail: vicens@unistra.fr*

Hyun Jung Kim

Hyun Jung Kim was born in Pohang, Korea in 1982 and received a BS (2005) and an MS Degree (2007) with chemistry major from Dankook University in Seoul, Korea. She subsequently received PhD degree in organic chemistry under the supervision of Prof. Jong Seung Kim at Korea University in 2011. Her main research interests concern 'molecular design and synthesis of chromogenic/fluorogenic sensors'. Her research publication records 40 reviewed papers and 10 patents so far.

Min Hee Lee

Min Hee Lee was born 1983 in Suwon, Korea and received her BS degree in 2006 and MS degree in 2008 majored in chemistry from Dankook University in Seoul, Korea. She then joined Prof. Jong Seung Kim's lab as a PhD student and involved in a project of 'chemosensors to detect specific ions via fluorescence and visual color changes'. Her research publication records 28 reviewed papers and 6 patents so far.

can expand the range of performance of existing chemicals and materials. Since the covalent bonds between atoms are precisely defined within dimensions lower than 1 Å, chemists have become accustomed to handling and constructing molecular objects on a very small scale. Ordering molecules chosen for a property on a surface, or self-assembled monolayers (SAMs), has become possible, thus giving rise to a new generation of chemical and biological sensors. SAMs guarantee the functionality of each molecule to function singly and carry out its own original functions.

Whitesides *et al.*[1] claimed that surfaces represent a fourth state of matter. Different from molecules in bulk, molecules at the surface of a material constitute a completely different environment with different free energies, electronic states, reactivity, mobility, and structures. SAMs constitute particular hybrid materials[2–7] that can be used in the construction of convenient, flexible, and simple systems to tailor the interfacial properties of metals, metal oxides, and semiconductors. SAMs are organic assemblies formed by the adsorption of molecular constituents from solution or the gas phase onto the surfaces of solids.

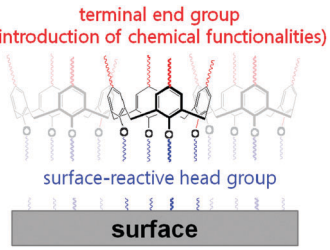

Calixarenes have been broadly exploited in all areas of supramolecular chemistry over the past three decades[8–11] and many recent developments have concerned their application in the production of chemical entities on a nanometre scale.[12] Calixarenes recently entered the nanoworld[13] and several recent reviews[14–24] have appeared reporting their supramolecular chemistry along with their ability to be involved in self-assembly processes for the construction of new nanomaterials.

This review focuses on the preparation, formation, structure and applications of luminescent SAMs based on solid supported calixarenes.

2. Gold-supported calixarenes

2.1. Principles

Gold nanoparticles (AuNPs) are hybrid organic–inorganic compounds characterized by a thick organic layer self-assembled on the surface of a core of gold atoms, having a nanoparticle size.[25] The SAMs of thiols on gold are key elements for the construction of many systems and devices with applications in the expansive field of nanotechnology.[26] When the dimensions of the gold are reduced to nanoscale, the optical properties are dominated by a collective oscillation of conduction electrons in resonance with incident electromagnetic radiation. This phenomenon is termed surface plasmon resonance (SPR). The surface plasmon absorption band, and consequently the color of a metal AuNP solution, is dependent on a number of parameters, the size and shape of the particle, the type of gold,

Lucia Mutihac

Lucia Mutihac received her PhD degree from Institute of Physical Chemistry of the Romanian Academy in Bucharest in the field of host–guest chemistry of amino acids and macrocyclic receptors in 1990. After several years as Senior Researcher within the same institute she was appointed Lecturer at the University of Bucharest in the Department of Chemistry. She is presently professor in Chemistry at the same University. Her research interests concern molecular recognition of biological compounds, transport through membrane and biomembranes, supramolecular chemistry. She is author/co-author of 150 reviewed publications and 1 patent.

Jacques Vicens

Jacques Vicens completed his PhD in 1977 at the Université Louis Pasteur (ULP) de Strasbourg in France. Then, in 1978, he got a first postdoctoral position in Belgium at the Université Notre-Dame de Namur. In 1980, he was awarded a second post doctoral position at the Weizmann Institute at Rehovot in Israel. Then he entered the Centre National de la Recherche Scientifique in 1981 at the Université Claude Bernard de Lyon in France. In 1988, he joined back the Université de Strasbourg. Dr Vicens is author/co-author of 350 reviewed publications and 2 patents.

Jong Seung Kim

Jong Seung Kim was born in Daejon, Korea in 1963. He received PhD from Department of Chemistry and Biochemistry at Texas Tech University. After one-year postdoctoral fellowship at University of Houston, he joined the faculty at Konyang University in 1994 and transferred to Dankook University in 2003. In 2007, he then moved to Department of Chemistry at Korea University in Seoul as a professor. To date, his research records 270 scientific publications and 25 domestic and international patents.

the dielectric properties of the medium, and the distance between particles.[27–30] AuNPs, with an interparticle distance greater than the average particle diameter, appear red as a consequence of the surface plasmon absorption band centered at 520 nm. As the interparticle distance decreases to less than the diameter of the particles, coupling interactions induce a broadening and a shift to longer wavelengths of the surface plasmon absorption band, which results in a solution of aggregated AuNPs that appears blue. Using SPR and the color change of AuNPs, specific guest molecules in environmental and biological fields can be selectively detected and separated.[31] Here, a novel molecular recognition system using a calixarene derivative has been applied to an AuNP sensor.

2.2. Cation sensors

Koh *et al.* provided a significantly useful method for K^+ sensing with high sensitivity and selectivity using SAMs of calix[4]crown-5 derivative (**1**) or Prolinker™ modified gold chip based on SPR.[32] In order to confirm the formation of calix[4]crown-5 SAM on the gold chip surface, SPR, cyclic voltammetry (CV),[33] atomic-force microscopy (AFM),[34] and Fourier transform infrared reflection absorption spectroscopy (FTIR-RAS)[35] were conducted. The SPR angle shifts were steadily increased and saturated within 5 h. Particularly, $\nu(sp^2$ C–O) stretching at 1203 cm^{-1} confirmed the presence of the crown-ether group on the gold surface. The compound **1** monolayer exhibited a more sensitive and selective sensing toward the K^+ ion over other alkali and alkaline earth metal ions. Fig. 1 shows that the SPR angle shift is 0.38° at the highest concentration of the K^+ ion (0.01 M), which is more than four times greater than that of other ions. The interaction between **1** and the K^+ ion enables us to selectively sense the K^+ ion in a broad linear range of 1.0×10^{-12} to 1.0×10^{-2} M by SPR. Moreover, even at the lowest detection limit, 1.0×10^{-12} M, the angle of SPR is substantially changed to 0.13°, which is approximately two times that of other ions at the same concentration, which remains below 0.067°. These results are caused by the strong host–guest interaction between the K^+ ion and the well-formed calix[4]crown-5 derivative monolayer. It was determined that system **1** had a higher SPR response over the near-neutral pH range from 6 to 8, which indicates that the K^+ sensing system can be successfully applied to biological systems.

Another example of an ion-selective SAM modified receptor with calix-crown, 1,3-alternate 25,27-bis(11-mercapto-1-undecanoxy)-26,28-calix[4]benzocrown-6 (**2**), was reported by Dabestani *et al.*[36] The sensor can detect caesium ions in the range of 10^{-12}–10^{-7} M concentrations and shows potential for use in the development of a new family of real-time *in situ* metal ion sensors with high sensitivity/selectivity and low cost, for chemical and biological applications. As shown in Fig. 2, the most impressive response is exhibited when the concentration of caesium ions is in the range of 10^{-7}–10^{-11} M. In contrast, the response to potassium ions in the same concentration range is quite small. The bending response of the **2**-SAM-coated microcantilever upon Cs^+, K^+ and Na^+ complexation was compared for the same concentration of each ion (10^{-5} M). The results indicated that the **2**-SAM-coated microcantilever was much more selective towards Cs^+ ions over K^+ and Na^+ ions. The results of the study demonstrate that the concept of ion-selective SAM-coated cantilever can be applied efficiently to sense trace amounts (ppb) of caesium ions (*in situ*) in the presence of high concentrations of interfering K^+ and Na^+ ions with remarkable sensitivity.

Another incorporation of calix[4]crown-6 derivatives, **3** and **4**, into SAMs to study their ion recognition properties has been previously reported by Zhang and Echegoyen.[37]

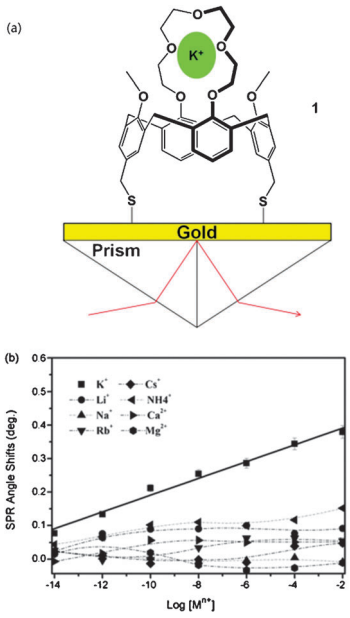

Fig. 1 (a) A sensor chip configuration. (b) SPR angle shifts with respect to various concentrations of several metal ions. Solid line is the linear fit (r^2 = 0.9928). Other lines were used to guide eyes.

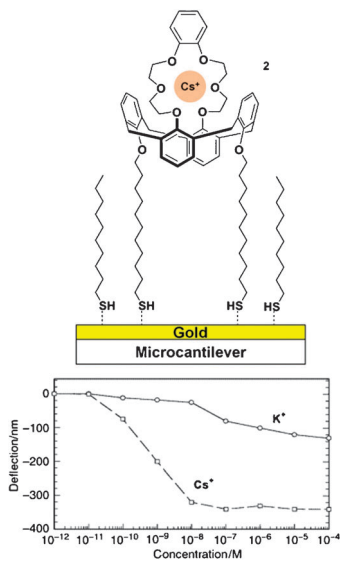

Fig. 2 (a) Molecular structure of **2** co-absorbed with decane-1-thiol on the gold surface of a microcantilever *via* the SAM technique. (b) Bending deflection response of the SAM-coated microcantilever as a function of the change in the concentration of Cs^+ and K^+ ions. For the *y*-axis, the voltage has been converted to nm using the conversion factor 10.58 mV nm^{-1}.

Two conformational isomers of bis-thioctic ester derivatives of *p-tert*-butylcalix[4]crown-6, **3** (1,3-alternate) and **4** (cone) form stable SAMs on the gold surface. **3** evidenced reversible and selective complexation with Cs^+ ions. Upon the addition of 45 mM CsCl to the **3** modified electrolyte, cathodic current is reduced drastically and the corresponding anodic current is almost completely disappeared. This observation is ascribed to the suppression of electron transfer at the interface as the consequence of strong repulsion between the calixcrown-bound cations and the positively-charged $Ru(NH_3)_6^{3+/2+}$ redox couple. In contrast, the CV response at the **4** modified gold electrode shows almost no change upon the addition of CsCl to the electrolyte. This indicates that **4** cannot bind to Cs^+, but that **3** can detect the caesium ion very efficiently. This Cs^+ selectivity of **3** must be controlled by two factors: proper size of crown ether for Cs^+ ion, and a cation–π interaction between the Cs^+ ion and two calix[4]arene aromatic rings.[38] The sensing abilities of the SAMs of **3** and **4** for other cations were also tested. However, negligible changes in the value of R_{ct} were noted for Na^+ and K^+, respectively, suggesting that neither Na^+ nor K^+ can form stable complexes with SAMs of **3** or **4**.

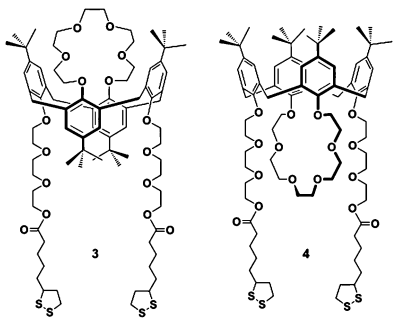

Echegoyen *et al.* also reported the synthesis, SAM formation and characterization, and metal cation recognition properties of three conformational isomers of bis-thioctic ester derivatives of *p-tert*-butylcalix[4]crown-6, cone **5**, 1,3-alternate **6** and partial-cone **7**.[39] Additionally, one bis-thioctic ester derivative of *p-tert*-butylcalix[4]arene (**8**) was also synthesized. The SAMs of these compounds were prepared and characterized *via* electrochemistry, reflection–absorption infrared spectroscopy (RAIRS) and contact angle measurements. The binding properties of the SAMs of these compounds with metal cations were systematically investigated *via* electrochemical techniques and impedance spectroscopy. The addition of Ba^{2+} to the SAMs **7**-modified electrolyte results in a drastically reduced cathodic current, from 8.9 μA in the absence of Ba^{2+} to 4.3 μA in the presence of 60 mM Ba^{2+}. Similarly, drastically reduced faradic currents were observed after the addition of Ca^{2+} to the same gold electrode.

On the other hand, the CV response at a **7**-modified gold electrode in the presence of K^+, Na^+ or Cs^+ evidences almost no change. These results show that **7** can bind to Ba^{2+} and Ca^{2+}, but does not effectively bind with alkali metal cations. All the SAMs built with **5–8** serve as good sensors for Ca^{2+} and Ba^{2+}, as confirmed by CV blocking experiments and impedance spectroscopy.

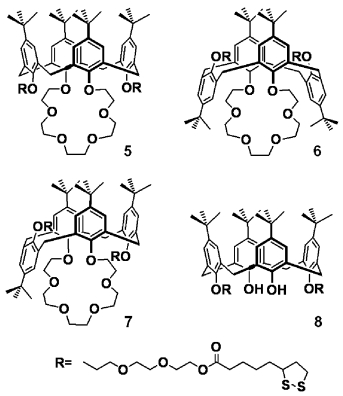

A wavelength interrogation SPR sensor with gold substrate modified with a calix[4]arene derivative (**9**) was used to detect metal ions in aqueous solutions. It was demonstrated that sulfur containing calixarene derivative SPR sensors could selectively discriminate Ag^+ and Cu^{2+} from some other metal ions by Chen *et al.*[40] The Au–S bond between the calixarene derivative and the gold substrate was confirmed *via* X-ray photoelectron spectroscopy (XPS) data. In order to evaluate the selectivity of sulfur-containing calixarene derivatives **9** and **10**, gold substrates modified with **9** and **10** were used, respectively. According to the resonant wavelength shift, it was determined that Cu^{2+} and Ag^+ could be detected by sensing films modified with **9** and **10** over a range of concentrations. On the other hand, no significant SPR responses were noted for other ions, even at high concentrations (0.01 M). The detection limit of calixarene derivatives as a sensing film for Ag^+ (10^{-7} mol L^{-1} for **9**, 10^{-6} mol L^{-1} for **10**) was lower than that for Ag^+ when thiol was used as a sensing film (10^{-4} mol L^{-1} for thiol). This proved that the calixarene skeleton played an important role in the detection of Ag^+ of low concentrations of the SPR sensor. As further proof, in the presence of K^+, Na^+, Mg^{2+}, Ca^{2+}, Fe^{2+}, Co^{2+}, and Zn^{2+}, no characteristic peaks for these ions appeared on the XPS spectra. For **9**, the detection limit of Ag^+ (10^{-7} mol L^{-1}) was lower than that of Cu^{2+} (10^{-4} mol L^{-1}). This means that the determination of Ag^+ will not be disturbed by Cu^{2+}, provided that the concentration of Cu^{2+} is below 10^{-4} mol L^{-1}.

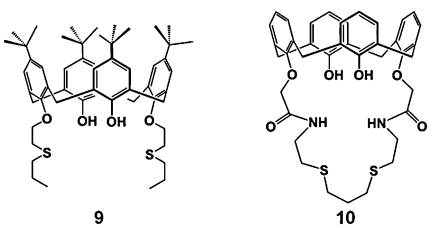

An and Zhong *et al.* described a AuNPs-based strategy for cationic detection using structurally-tailored **11**.[41] Compound **11** shows a *cone*-conformation based on ^1H NMR patterns arising from the $ArCH_2Ar$ methylene protons. Upon the addition of K^+, Ba^{2+} and Pb^{2+} to the solution of Au@**11**, the surface plasmon band evidenced reduced absorbance at

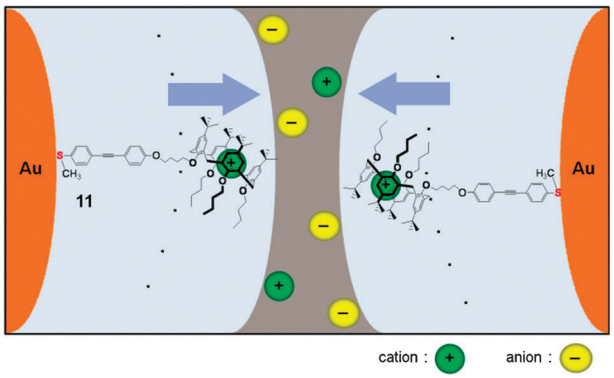

Fig. 3 A proposed mechanism for the interparticle interaction as a result of binding of M^{n+} into **11**, formation of an electrical double layer, and aggregation of the charged nanoparticles.

533 nm with an increase at 620 nm. The increase of absorbance at 620 nm for the case of Pb^{2+} appeared far more significant than those for K^+ and Ba^{2+}. For the addition of Cu^{2+}, Ca^{2+}, and Cs^+, the surface plasmon band showed a red shift to 650–800 nm. Among these cations, Cs^+ showed the largest red shift (750 nm) in the absorbance band. The aggregation of AuNPs upon addition of the cations is responsible for the optical change in the surface plasmon band. Control experiments also included the addition of Na^+ or Li^+ into the solution of Au@**11** and showed no changes in the surface plasmon band characteristics, demonstrating the ionic selectivity of the nanoprobes. The simulation of the red shift of the surface plasmon band was based on the comparison with those for Au@**11** in response to the addition of Cu^{2+} (Fig. 3).

2.3. Anion sensors

Two anion receptors based on **12** and **13** were synthesized and characterized previously by Echegoyen *et al.*[42] To obtain insight into the binding mode of receptors **12** and **13** with fluoride ions, ^{1}H NMR measurements were performed. The results indicate that receptors **12** and **13** evidence the highest binding affinity for fluoride ions over other anions, including Cl^-, Br^-, NO_3^-, HSO_4^-, $H_2PO_4^-$, and AcO^-. SAMs of **12** were formed on gold surfaces and characterized *via* reductive desorption and other techniques. CV and electrochemical impedance spectroscopy were used to monitor anion sensing by the SAM-modified gold electrodes. Upon the addition of the F^- anion, the gold electrodes modified by SAMs of **12** evidenced a dramatic increase in charge-transfer resistance (R_{ct}) values. This is due to the electrostatic repulsion between the negatively-charged electrode surfaces and the negatively-charged $Fe(CN)_6^{3-/4-}$ redox probe in the electrolyte solution. A dramatic fluorescence spectral change was noted upon the addition of F^- and AcO^- to **13**. In contrast, the fluorescence of **13** with various anions such as Cl^-, Br^-, NO_3^-, HSO_4^-, and $H_2PO_4^-$, led to essentially no change in excimer emission and a slight enhancement of monomer emission.

2.4. Biomolecule sensors

To explore the potential applications of calixarenes as ammonium sensors, Echegoyen *et al.* decided to prepare suitable receptors based on calix[6]arene.[43] Compound **14**, with a rigid cavity immobilized on gold surfaces *via* self-assembly, can function as a remarkably efficient aniline sensor. The binding abilities between the SAMs of **14** and the alkylammonium cations are not very strong, as the observed current reduction is not very pronounced. In contrast, the addition of anilinium chloride to the SAMs of **14** electrolyte results in a drastic reduction in both cathodic and anodic currents. This indicated that the SAMs of **14** evidenced a marked recognition ability for anilinium chloride relative to alkylammonium cations. The remarkably efficient recognition of anilinium chloride by SAMs of **14** is probably attributable to the good size fit between the calix[6]crown-4 cavity and the aniline. Cation–π interaction, hydrophobic interaction, and CH_3–π and π–π stacking between anilinium and the host monolayer may contribute to molecular recognition. From these results, they also studied the binding affinity of **14** toward other biogenic amines, such as dopamine. Dopamine is one of the most important neurotransmitters. CV blocking experiments and impedance spectroscopy demonstrated that SAMs of **14** exhibit much better recognition for dopamine than for the alkylammonium salts (Fig. 4).

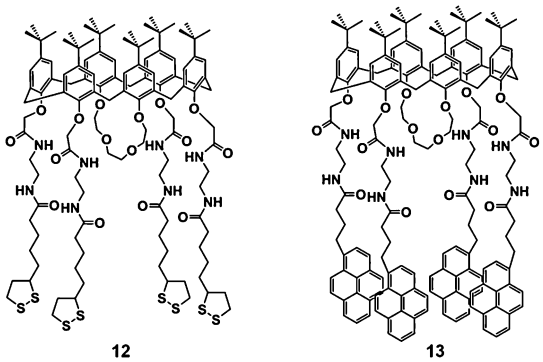

Patel and Menon report a concept for amino acid recognition by **15** attached nanoparticles in which the recognition of a given amino acid triggers particle aggregation *via* simple electrostatic interactions and induces an easy-to-read color change.[44] This report focuses principally on the synthesis of very stable, yet chemically versatile, novel, and water-soluble **15**, and its application as a novel colorimetric sensor for lysine (lys), arginine (arg) and histidine (his) from red to purple. The absorbance spectrum of the Au@**15** solution shows an absorption maximum at 524 nm. To investigate the amino acid recognition ability of novel Au@**15**, 11 different amino acids were added to Au@**15**. 30 min later, the Au@**15** solutions containing lys, arg or his

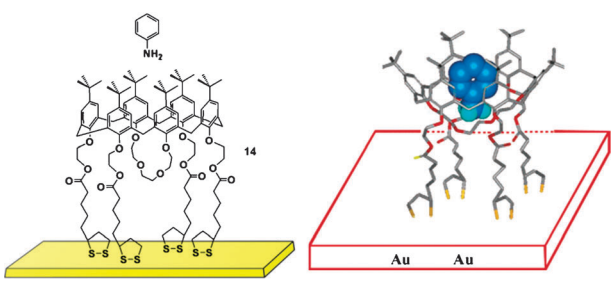

Fig. 4 Gold-supported calixarene **14**.

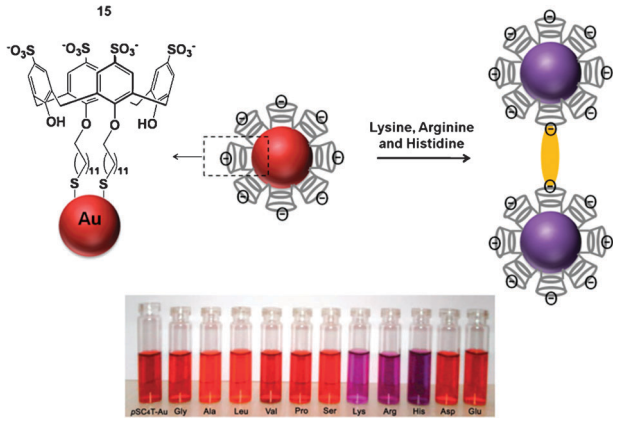

Fig. 5 A schematic representation of the amino acid-induced aggregation of Au@**15**.

had changed color from red to purple (Fig. 5). Upon the addition of amino acid, a red shift in the wavelength (524 nm to 550 nm region) and a broadening of the surface plasmon band occurs, which is accompanied by the aggregation of Au@**15**. Control experiments of **15** alone without AuNPs showed no peaks in the 550 nm region in the presence and absence of amino acids. They also evaluated the stability of the AuNP–calix assembly in different ranges of pH. These AuNP–calix assemblies evidenced less stability and were aggregated within a few minutes in low pH solutions from 2 to 4. However, the AuNP–calix assemblies were very stable in solutions from pH 6 to 10 at elevated temperatures, for weeks to months with no aggregation.

Using calix[6]arene provided with thiols, SAM electrodes were prepared, and the electrode reaction of catecholamines on bare gold electrodes and the SAMs electrodes were investigated in a previous study by Nakano and Shinkai *et al.*[45] It was found that **16** partly blocked the electrode reaction of dopamine in the solution phase. In the case of 3,4-dihydroxy-DL-alanine (DOPA), this blocking effect was also observed only slightly. However, the electrode reaction of 3,4-dihydroxyphenylacetic acid (DOPAC) was almost completely inhibited. These results imply that dopamine and DOPA (as cationic substrates) bound with the thiol-appended calixarene molecules on the electrode surface and induced a Faradaic reaction with the underlying gold electrode. The thiol-appended calixarene molecular-pore was expected to function as a spatial pass for electron transfer, resulting in a feasible electrode reaction. The authors also described a possible application to an electrochemical dopamine sensor.

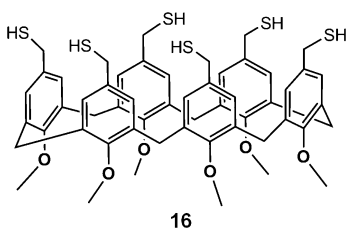

16

Veggel and Reinhoudt *et al.* reported on SAMs on AuNPs of calix[4]arene ± resorcin[4]-arene (2 : 1) receptor **17** equipped with four didecyl sulfide groups.[46] These monolayers were confirmed *via* contact angle measurements, polarized infrared external reflectance spectroscopy (PIERS), electrochemical capacitance and resistance measurements, and XPS. The interaction between monolayer-**17** and steroid guests was evaluated *via* SPR spectroscopy. The SPR data show that steroids interact more strongly with a monolayer of **17** than with a hydrophobic reference monolayer of octadecanethiol, and no detectable interaction with a hydrophilic reference monolayer of 11-mercaptoundecan-1-ol was observed. The higher responses obtained for the monolayer of **17** are probably due to the overall structure of the layer: a combination of specific steroid receptors and voids which provides the receptors with space to adapt to the guest molecules, and permits guest intercalation between the receptor molecules.

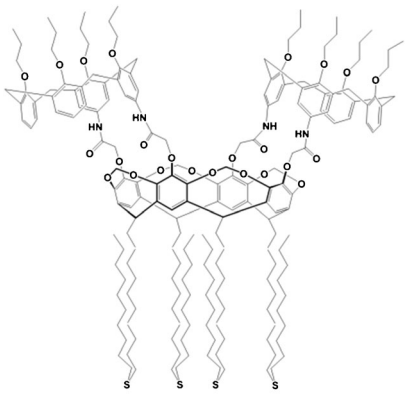

17

Koh *et al.* prepared SAMs of the carboxylic acids calixarene (**18**), ProLinker™ (already known for its complexation properties of proteins), at the lower rim and reactive thiol at the upper rim.[47] The characterization of SAMs of **18** was monitored *via* FTIR-RAS, AFM and CV. The surface coverage on Au was determined to be 6.647×10^{-11} mol cm^{-2} for **18**. The estimated surface concentration of bovine serum albumin (BSA) by SPR was the largest for ProLinker™ with an

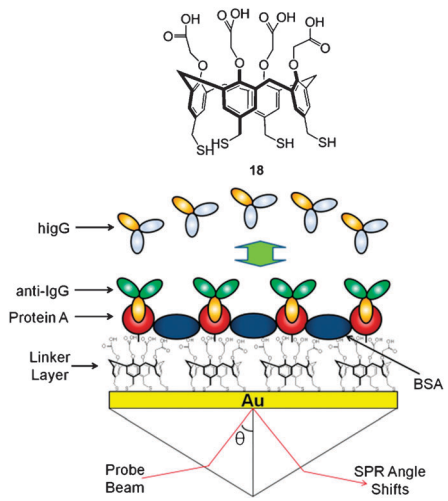

Fig. 6 Schematic diagram of protein–protein interaction between hIgG and anti-hIgG on **18** linker system confined Au surface.

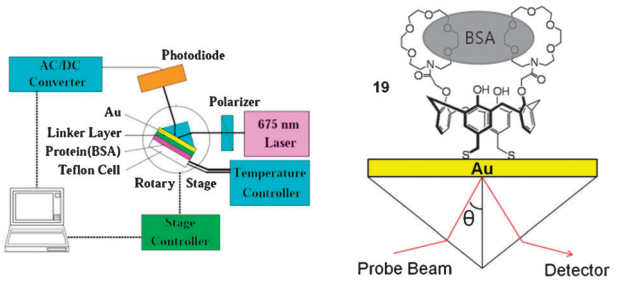

Fig. 7 Schematic diagram of the homemade SPR system and a sensor chip configuration.

excellent immobilization of BSA. The same SAMs were used to show evidence by SPR of protein–protein interactions using anti-hlgG and hlgG at very low concentrations (Fig. 6).

Koh *et al.* described the formation of SAMs of calix[4]bisazacrown (**19**) and commercial ProLinker™ on AuNPs.[48] Due to the presence of crown moieties, ammonium groups of proteins can be complexed, allowing for the immobilization of BSA. The linkage was monitored *via* the SPR technique. The surface concentration of BSA calculated by the simulation of SPR experimental data was higher for the **19** (197 ng cm^{-2}) than for the ProLinker™ (175 ng cm^{-2}). This difference was explained by a stronger binding due to hydrogen bonds between ammonium groups of BSA and the nitrogen atom of the azacrown loops (Fig. 7).

2.5. Other sensors

Li *et al.* reports the synthesis of Au@**20** in aqueous media for the colorimetric detection of diaminobenzene (DABs) isomers.[49] The Au@**20** were characterized *via* IR spectroscopy, ultraviolet–visible spectroscopy (UV-vis), transmission electron microscopy (TEM), *etc.* The color of the Au@**20** solution is red because of the intense surface plasmon absorption band centered at 520 nm. The electrostatic interaction and host–guest interaction between Au@**20** and DABs induce the aggregation of the nanoparticles. Upon aggregation, the surface plasmon absorption band red-shifts and broadens so that the nanoparticle solution exhibits a deep purple color. Interestingly, as shown in Fig. 8, the color changes of DAB isomers differ profoundly. In 30 min, the solution containing *m*-DAB and *p*-DAB changes from red to purple, and the characteristic absorption peaks of the solution containing *m*-DAB and *p*-DAB shift from 520 to 532 nm. However, the solution containing *o*-DAB exhibits neither a color change nor an absorption peak shift. These results imply that the Au@**20** responded selectively to *m*-DAB and *p*-DAB, but not to the *o*-DAB. The Au@**20** aggregation induced by these two DAB isomers is supported by the TEM images, which show that *p*-DAB induced greater Au@**20** aggregation than *m*-PAB. The sensitivity of Au@**20** towards other amines, including *o*-diaminobenzene, *o*-nitroaniline, *m*-nitroaniline, *p*-nitroaniline, *o*-chloroaniline, *p*-chloroaniline, *o*-toluidine, *m*-toluidine, *p*-toluidine and aniline, are negligible.

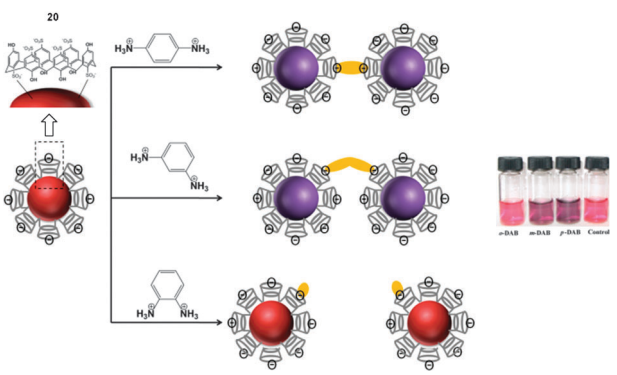

Fig. 8 Schematic representation of the isomeric DABs induced aggregation of Au@**20**.

The 1,3-dialkoxycalix[4]arenes are known to form endocavity inclusion complexes with quaternary ammonium cations.[50] To reveal a possible effect of the calixarene cavities' distance from the gold core on the recognition efficiency, calix[4]arenes (**21**) bearing two alkanethiol chains of six or eleven carbon atoms were prepared by Pochini *et al.* Analysis of the results clearly demonstrates that the introduction of calix[4]arene recognition elements with a C6 linker onto the monolayer protected cluster surface increases the extent of binding of *N*-methylpyridinium tosylate. The binding efficiency is enhanced gradually as the number of calixarene units present on the gold nanoparticle increases. The length of the two thiol chains that function as spacers between the 1,3-dithioalkoxycalix[4]arenes and the nanoparticle surface largely affect the extent of binding affinity. As a consequence, the nanoparticles derived from **21** ($n = 6$) show a further enhancement in the binding efficiency. For instance, the binding constant calculated for **21**, in which the dodecanethiol chains are completely substituted, is three orders of magnitude higher than that experienced by 1,3-dialkoxycalix[4]arenes without thiols. These data clearly demonstrate that clusters of calixarene hosts supported on a gold nanoparticle are very efficient receptors for the recognition of ammonium cations (Fig. 9).

It is well known that host molecules including calix[4]-, calix[5]-, calix[6]-, and calix[8]arenes form stable complexes with C_{60} and/or C_{70}. Echegoyen *et al.* report the use of the noncovalent interaction between calix[8]arene receptors and fullerenes to immobilize C_{60} on surfaces.[51] One calix[4]arene derivative, three calix[6]arene derivatives, and one calix[8]-arene derivative **22** with surface anchoring groups were synthesized and characterized completely by ^{1}H and ^{13}C NMR

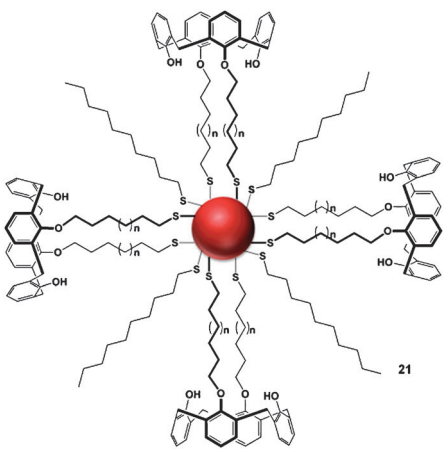

Fig. 9 Gold-supported calixarenes **21**.

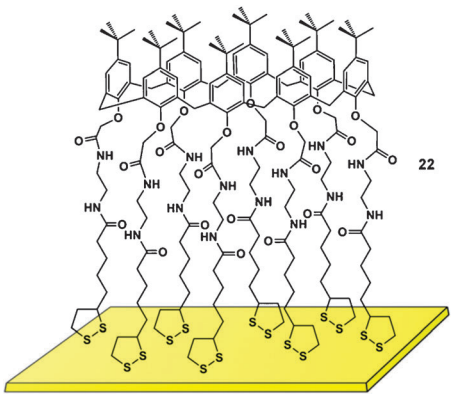

Fig. 10 Gold-supported calixarene **22**.

and MS spectroscopies. **22** provides a better size fit for complexation of C_{60}, as compared to calix[*n*]arene derivatives ($n = 4, 6$). The SAMs of calix[*n*]arene derivatives ($n = 4, 6$) evidenced no ability to bind to C_{60} on the gold surfaces. After incubation in the C_{60} solution, the peak currents of SAM-modified electrodes with **22** were gradually reduced upon successive scans, thereby indicating the dissolution of C_{60} and/or the desorption of the monolayers (Fig. 10).

3. Silver-supported calixarenes

3.1. Principles

As mentioned above, the combination of the physical properties of nanostructured metals[52–54] and the advanced chemical properties of self-assembled calixarenes are of current interest in supramolecular chemistry, with several applications in chemical sensing, environment, and nanotechnology. The introduction of receptors onto nanoparticle surfaces has provided not only stability in various solvents, but also desirable surface functionality.[55] Following the discovery of the remarkable antitumoral, antibacterial, anti-inflammatory, and wound healing properties of silver nanoparticles (AgNPs),[56,57] these materials have been modified using different macrocycles, including crown ethers,[58] cyclodextrins,[59] cucurbiturils,[60] or calixarenes,[50] and further employed as hosts in the molecular recognition of various compounds, as well as for developing new methods in chemical and biological fields.[61,62]

Generally, colloidal AgNPs are prepared using hydroxylamine hydrochloride as a reducing agent.[63] These nanoparticles have the advantage of a more uniform distribution of size and shape along with the absence of reducing agent (citrate or borohydride) excess, which could interfere with the surface-enhanced Raman scattering spectroscopy (SERS) measurements.[64] The AgNPs suspension, characterized by the resonance spectra of metallic plasmons, evidences a maximum at ~410 nm with an average full width at a half-height of 80 nm.[65] Moreover, these chloride-covered nanoparticles evidence better electrochemical properties on the surface and improved adherence properties, which facilitates their immobilization on glass by simple deposition. Subsequent to the immobilization of AgNPs, either in suspension or immobilized on glass, their covering by adsorbed self-assembled calixarene molecules follows. By potential-sweeping electro-deposition of calixarene-modified AgNPs on glassy carbon electrode in one-step, an electrochemical sensor can be created.[66]

3.2. Aromatic hydrocarbon sensors

Polycyclic aromatic hydrocarbons (PAHs) with condensed benzene rings are important environmental pollutants.[67] They can be found as a mixture of differently-related molecular compounds in air, soil, and water due to natural processes and human activity. Their detection by surface-enhanced techniques is limited because these molecules evidence low affinity for adsorption on a metallic surface. By using calix[4]arene derivatives as self-assembled molecules adsorbed on AgNPs, Sanchez-Cortes *et al.*[68,69] selectively detected PAHs (Chart 1) in trace concentrations *via* SERS.

In this regard, nonthiolic calixarenes, such as 25,27-carboethoxy-26,28-hydroxy-*p*-*tert*-butylcalix[4]arene (**23**) as a host molecule, have been employed for the functionalization of a metal surface in the design of a film for optical sensing.[68] This host molecule evidences analytical selectivity to the PAHs bearing four benzene rings, principally pyrene (Chart 1). Thus, trace concentrations of PAHs have been detected using surface-enhanced Raman scattering spectroscopy. Hence, new SERS substrates have been developed that consisted of Ag nanoparticles in suspension or nanoparticles immobilized on glass and covered by adsorbed self-assembled calix[4]arene molecules. Some authors have suggested that the host–guest interaction mechanism occurs *via* a π–π staking interaction, leading to a charge transfer between the complex and the metallic surface, which could have some influence on the surface charge of the metallic nanoparticle. Fig. 11, which evidences normalized areas corresponding to the SERS bands of different PAHs studied, shows that all four-ringed assayed PAHs (PYR, TP, and BcP) evidenced enhanced selectivity. In contrast, the larger PAHs (COR, RUB, and DBA) exhibited the lowest SERS intensities. The size specificity is likely to be determined by the cavity of the calixarene and the *tert*-butyl groups placed in the upper rim. These results led to the conclusion that the binding properties of each PAH must vary as a function of its chemical structure, highlighting the size and shape selectivity of **23** in interactions with PAH molecules.

Calixarenes harboring a dicarboethoxy ($–CH_2–CO_2Et$) substituent at the lower rim are good receptors in the design of highly sensitive and selective optical sensors of PAHs-based

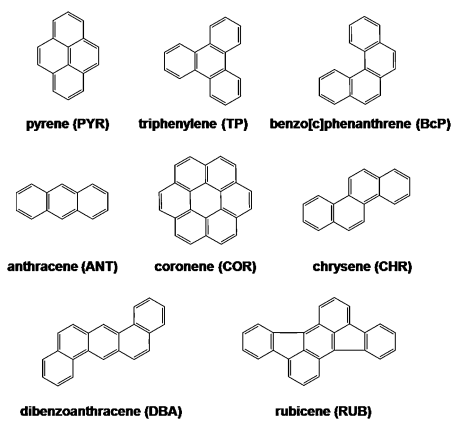

Chart 1 Polycyclic aromatic hydrocarbons.

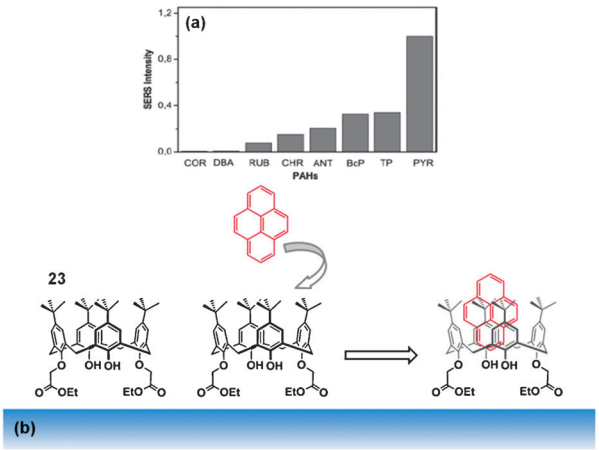

Fig. 11 (a) Normalized areas (with respect to the 1405 cm^{-1} band of PYR in the complex with **23**) of the most intense SERS bands of the studied PAHs (10^{-4} M) on **23** (10^{-4} M). All of the intensities were registered by excitation at 1064 nm. (b) Host/guest complex on the surface.

vibrational spectroscopy. **23** was found to have a higher affinity for PYR and BcP. The studies continued with surface-enhanced micro-Raman spectroscopy (micro-SERS), which was used to reduce the molecular detection limits of PYR and BcP deposited onto a calix[4]arene-functionalized AgNPs.[69] Good reproducibility and low molecular detection limits (10^{-8} M) were obtained. Silver films prepared by immobilizing hydroxylamine-reduced AgNPs were sensitive when applied in micro-SERS detection, yielding reproducible results. By changing the amount of potassium nitrate added to the suspension, the morphological properties of the AgNPs aggregates can be modulated. The SERS spectra of the complexes calixarene–PAHs at different host and guest concentrations led to the conclusion that the best micro-SERS spectrum of the compounds should be obtained at relatively low concentrations of the host molecule, rather than the opposite. The detection limit was much lower in the case of benzo[*c*]phenanthrene than in pyrene when excited with the 785 nm line of a diode laser. It was suggested that benzo[*c*]phenanthrene induced a stronger effect on the adsorbed calixarene because of its non-planar structure, which is induced by the presence of bay-like moieties.

Based on the ability of the dithiocarbamate (DT) group to interact strongly with the surfaces of metals by forming chelate complexes,[70] the combination of host properties of calixarenes and the high affinity of the DT group in the same molecule, self-assembled on a nano-structured metal has led to design-sensitive and selective surfaces for the detection of PAHs (Chart 1). As such, the synthesis of 25,27-diethyl-dithiocarbamic-26,28-dihydroxy-*p*-*tert*-butylcalix[4]arene (**24**) aiming at increasing the affinity of the calixarene host toward nanoparticle surfaces and the detection of pyrene by surface-enhanced Raman scattering using **24** in the functionalized of AgNPs was previously reported by Sanchez-Cortes *et al.*[71] A host–guest interaction mechanism based on a π–π staking interaction has been assumed, in which pyrene adopts a perpendicular orientation with respect to the surface. Pollutants were also detected at trace concentrations.

As a consequence of AgNPs functionalization with **24**, a sensitive and selective supramolecular host was realized for quantitative study in water of four PAHs: pyrene, triphenylene, benzo[*c*]phenanthrene (BcP), and coronene (COR) (Chart 1) detection using SERS.[72] It is worth mentioning that by means of a **24**-NPs system, the SERS detection of PAHs directly in the aqueous AgNP suspension was allowed, which was not possible in AgNPs functionalized with other kind of calixarenes. Through the S atoms of **24**, the adsorption of **24** on the nanoparticles is achieved by a transformation of the dithiocarbamate group into the corresponding thiouride form,[70,73] which was disclosed by the new band around 1520 cm^{-1} attributed to the stretching of the partial $C{=}N^{+}$ double bond.

A host–guest interaction mechanism through π–π staking between the aromatic part of **24** and PAHs results in the formation of a charge-transfer complex. The sizes of these pollutants range from four to seven condensed benzene-rings. The analysis of the SERS spectrum of **24** revealed marker bands associated with the binding of **24** to the metal ($\nu C{=}N^{+}$ and $I_{\nu(C=S)}/I_{\nu(C-S)}$ ratio), which suggests an increase in the bidentate interaction of calixarene adsorbed on the surface when the **24**-PAHs complex is formed (Fig. 12).

Considering the I_{702}/I_{665} ratio as a marker parameter of the cavity conformation, the conformational state of the aromatic intramolecular cavity was studied by assessing the I_{702}/I_{665} ratio, and the orientation of aromatic rings with respect to the surface was investigated by analyzing the I_{702}/I_{571} ratio. It was suggested that the intramolecular cavity seemed to adopt a closer configuration in the presence of the guest in the case of smaller I_{702}/I_{665} ratios, whereas at larger I_{702}/I_{571} ratios, the orientation of the benzene rings on the metal surface became

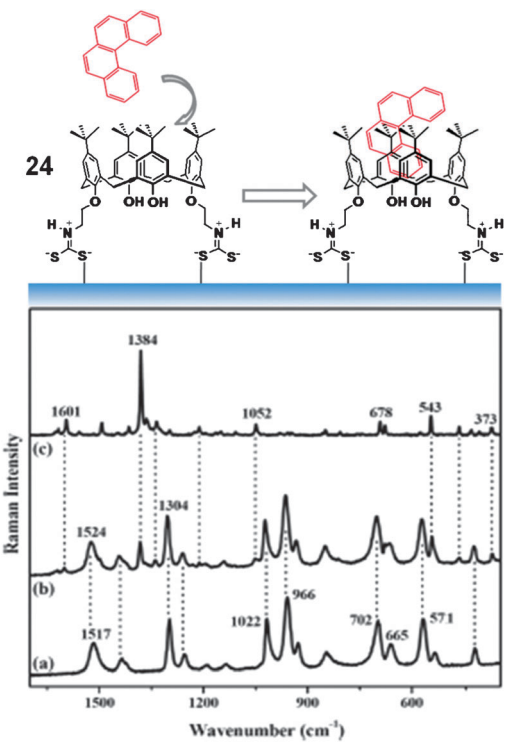

Fig. 12 SERS spectra of (a) **24** (10^{-4} M) and (b) **24**/BcP (10^{-4}/10^{-6} M). (c) Raman spectrum of BcP in the solid state. Excitation at 785 nm. Top scheme: structural change induced by the interaction of BcP with **24**, as deduced from the SERS spectra.

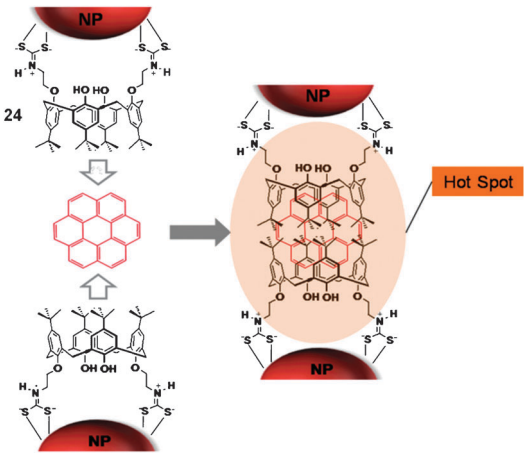

Fig. 13 Scheme showing the COR-**24** complexation mechanism with formation of the highly sensitive interparticle junction.

more perpendicular. Apart from COR, the affinity constants of Ag@**24** and pollutants (pyrene, triphenylene, BcP) evidenced similar behavior with regard to the interaction with the calixarene, and a limit of detection was determined for each pollutant in a range from 10^{-7} M to 10^{-8} M.

The higher affinity of COR relative to **24** and the lower influence on the calixarene structure have led the authors to propose the complexation mechanism shown in Fig. 13. In this host–guest complex, the host functions as a bridge between two calixarene molecules with the formation of highly sensitive inter-particle hot spots. The multicomponent analysis of pollutants by SERS depends on different factors, all of which should be studied in greater detail.

3.3. Organophosphorus sensors

The highly toxic effect of organophosphorus (OP) pesticides on human health is well known; this effect derives from the ability of these compounds to inhibit acetylcholinesterase. The development of new detection methods, more sensitive, highly selective, and running in real-time for OP pesticides in water is essential for chemistry, biochemistry, and environmental applications. Taking into account the molecular recognition abilities of water-soluble *p*-sulfonatocalix[4]arene (**25**) modified AgNPs towards some pesticides (iprodione, acetamipirid, thiabendazole, optunal, pyrimethanil, parathion-methyl, and methomyl, see Chart 2) in aqueous solution, a colorimetric sensor for optunal has been developed.[74]

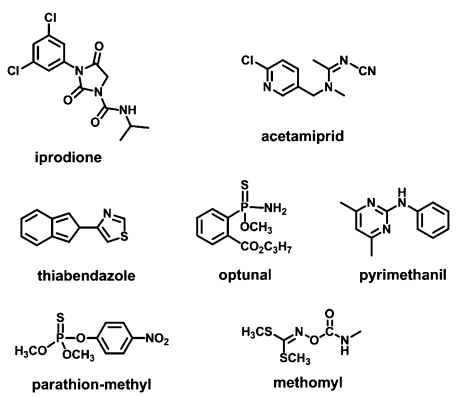

Chart 2 A series of pesticides investigated.

Compound **25** was obtained in water and characterized *via* TEM, FT-IR, and UV-Vis spectrometry. TEM images showed that both modified silver nanoparticles were highly dispersed and uniform in aqueous solution, with a diameter of approximately 8.0 nm.[74] Moreover, significant differences were detected in the FT-IR spectra of pure **25** and Ag@**25**, and particularly SO_3^-, which suggested that SO_3^- groups coordinated with silver atoms on the surfaces of AgNPs. The adsorption peaks of Ag@**25** originating from the surface plasmon absorption of silver NPs were detected at 393 nm. After the addition of pesticides to Ag@**25** solutions, the color turned from yellow to red, with increasing absorbance for optunal and Ag@**25**.

The selectivity of Ag@**25** toward optunal was attributed by the authors to the Ag@**25** aggregations induced by optunal, aspects of which are corroborated by the TEM images. A schematic representation of the optunal-induced aggregation of Ag@**25** is shown in Fig. 14. It is known that **25** binds to the aromatic and amino residues of optunal *via* host–guest interactions such as electrostatic forces, cation–π interactions, or π–π interactions. In brief, Ag@**25** can be utilized as a novel colorimetric sensor for optunal, allowing for the rapid quantitative assay of optunal down to a concentration of 10^{-7} M, which has potential ramifications for real-time *in situ* detection.

The *p*-sulfonatocalix[6]arene(**26**)-modified AgNPs were coated on glassy carbon electrodes (Ag@**26**/GCE) in view of the electrochemical detection of methyl parathion (MP, see Chart 2). Thus, a new electrochemical sensor based on modified AgNPs was realized *via* a one-step electro-deposition approach (Fig. 15).[66] Ag@**26**/GCE was characterized *via* attenuated total reflection IR spectroscopy (ATR-IR), XPS, and scanning electron microscopy (SEM). The MP detection was carried out with a detection limit of 4.0 nM. Even though the detection limit of this method was higher than the detection limits (0.1 nM,[75] 0.4 pM)[76] of the reported organophosphorus electrochemical sensors employing acetylcholinesterase, the stability and reproducibility of Ag@**26**/GCE were better than those of the enzyme-modified electrodes.

Compared with the AgNPs-modified electrode, the cathodic peak current of methyl parathion was amplified significantly. The simultaneous determination of MP was conducted *via* differential pulse voltammetry. A linear relationship between

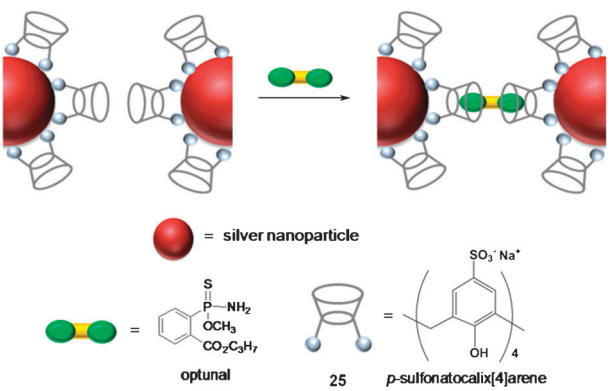

Fig. 14 Schematic representation of the optunal induced aggregation of Ag@**25**.

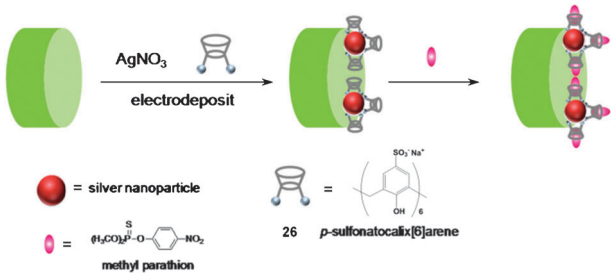

Fig. 15 Schematic diagram for one-step electrodeposition of Ag@**26** on the surface of the GCE for MP sensing.

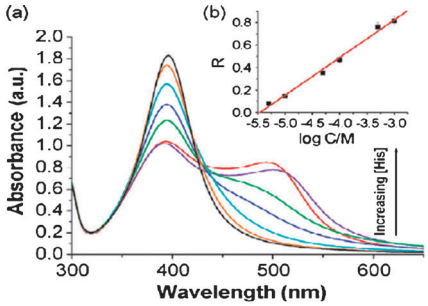

Fig. 16 (a) The adsorption spectra of Ag@**25** solutions with various concentrations of His (0, 5×10^{-6}, 10^{-5}, 5×10^{-5}, 10^{-4}, 5×10^{-4} and 10^{-3} M). (b) The dependence of the R (A_{493}/A_{394}) values of the pSC_4-AgNPs on increasing concentrations of His. Typically, 1 mL of various concentrations of His were added to 4 mL of Ag@**25** solution. The solutions were then mixed well for 30 min before being tested.

the current and MP concentration was obtained in the range of 0.01–80 μM. The well-defined cathodic peaks correspond to the irreversible reduction of $-NO_2$ to hydroxylamine groups. It was also observed that the peak current of MP measured by differential pulse voltammetry at Ag@**26**/GCE increased by 20 times compared with that obtained at the AgNPs/GCE, which confirmed that Ag@**26**/GCE exhibited good electrochemical catalytic activities toward MP. This could be explained as follows: hydroxylamine is partially protonated in neutral media, in cases in which **26** with its electron-rich cyclic cavity and the negative SO_3^- group can bind to the aromatic and hydroxylamine of MP *via* host–guest interactions such as electrostatic, cation–π interactions, and π–π interactions. Therefore, **26** binds to MP and simultaneously catalyzes the redox of MP.[66] The sensor was used for the determination of MP in pear samples and the recovery values ranged from 98.0% to 102.1%. It was demonstrated that the method can be used for the direct analysis of real samples with high accuracy, precision, and reproducibility.

3.4. Biomolecular sensors

A selective colorimetric sensor for histidine (His) in water, based on water soluble Ag@**25**, was reported by Li *et al.*[77] The Ag@**25** is stable in aqueous solution due to the macrocyclic effect. They were characterized by TEM, FT-IR, and UV-Vis spectroscopy. Noticeable differences were observed between the FT-IR spectra of **25** and Ag@**25**, and particularly for SO_3^-. Thus, the peaks for SO_3^- at 1187 and 1049 cm^{-1} found in pure **25** are shifted to 1178 and 1036 cm^{-1}, respectively, in Ag@**25**. Hence, it was suggested that the SO_3^- groups coordinate with the silver atoms on the surface of the AgNPs. The study of molecular recognition of Ag@**25** toward a series of amino acids (alanine, valine, leucine, methionine, phenylalanine, histidine, tyrosine, serine, proline, glutamic acid and aspartic acid) by UV–Vis with measurements after different reaction times has highlighted the selectivity of Ag@**25** to histidine in water. The changes in color appeared after the addition of 10^{-4} M solutions of various amino acids to Ag@**25** solution. Over 30 min, the solution containing histidine turned from yellow to red with an increase in the absorbance ratio A_{493}/A_{394}. The selectivity to histidine is attributed to the Ag@**25** aggregations induced by histidine, a hypothesis supported by TEM images. A linear correlation exists between R and concentration of histidine over the range of 5×10^{-6}–10^{-3} M.

The *p*-sulfonatocalix[4]arene (**25**) binds the imidazole and amino residue of histidine *via* electrostatic and cation–π interactions. These interactions between a histidine and two **25**-modified AgNPs result in Ag@**25** tending to aggregate more easily than the other amino acids tested. A schematic representation of the histidine-induced aggregation of the Ag@**25** process was suggested by the authors to be similar to that shown in Fig. 16[74] for optunal. This selective sensor allowed for a rapid quantitative assay of His down to a concentration of 5×10^{-6} M.

4. Silica-supported calixarenes

4.1. Principles

Hoffmann and Fröba[78] recently claimed that mesoporous organic–inorganic hybrid materials are an interesting class of materials, which combine the advantages of two worlds: the inorganic part builds a robust substrate, whereas the organic functions make them alive in a way that makes them potentially useful in a number of applications: catalysis, chiral walls, chiral sorption and catalysis, chromatography, enzyme immobilization, light harvesting, magnetic hollow nanoparticles, selective recognition of substrates and finally sensors.

A recent review by Jung *et al.*[79] presents the development of silica-based organic–inorganic hybrid nanomaterials as chromogenic and fluorogenic chemosensors for biological and environmental applications. This was achieved principally by grafting luminescent molecular probes on silica. These SiO_2-nanomaterials were capable of selectively detecting anions, neutral organic guests, and toxic metal cations.

With regard to calixarene-SiO_2 hybrid structures, previous studies have been conducted dealing with their supramolecular properties (host–guest chemistry). Katz and Iglesia *et al.*[80,81] immobilized *p-tert*-butylcalix[4]arene onto silica through activation of the silica surface by silicon tetrachloride *via* O–SiO_3 species. In this fashion, they obtained the highest coverage (207 μmol g^{-1}) on a per gram basis of materials reported for an immobilized calixarene. The surface is capable of guesting in calixarene cavity aromatic molecules such as phenol, benzene, toluene, and nitrobenzene. More recently, Guan and Jiang *et al.*[82] reported the formation of coaxial nanotubes of calixarene/silica *via* self-assembly and sol–gel transition. The calixarene was sophisticated calix[6]biscrown-4

harboring the NH_2 group assembled on silica using tetraethoxysilane. The obtained coaxial nanotubes were shown to complex with alkali cations with a preference for the caesium ion.

4.2. Metal ion sensors

Tran-Thi and Nicole *et al.*[83] have noticed that the sol–gel porous materials with tailored or nanostructured cavities have been increasingly used with regard to their potential as sensitive matrices or layers of chemical sensors for the detection of gaseous and ionic analytes. Such optical sensors are in full development in the environment, industry and health fields.[83] Recently, Jung and Shinkai *et al.*[84] reviewed the fabrication of a variety of silica nanotubes and their applications in environmental and biological fields since their discovery in the 1990's. Well-defined silica nanotubes can be obtained by simple sol–gel reaction, using self-assembled organogels as organic templates. This sol–gel transcription method has been shown to be very useful in creating new functional inorganic nanotubes. More particularly, they described recent advances in the detection and separation of heavy metal ions using colorimetric or fluorimetric systems. Silica nanotubes are useful as supporting materials for the fabrication of such functional hybrid nanomaterials by the sol–gel grafting method, due to the ease of covalent attachment of suitable functional organic molecules. The silica-based organic–inorganic hybrid nanotubes evidence high selectivity and sensitivity for specific toxic heavy metal ions, indicating that hybrid nanomaterials are useful as adsorbents to remove toxic environmental pollutants.

In this line of inquiry, and with respect to calixarenes, Jung and Kim *et al.*[85] described the preparation of functionalized silica organic–inorganic nanotubes (FSNT) possessing a pyrene-appended 1,3-alternate calix[4]arene (**27**) moiety as a fluorescent receptor and fabricated *via* the sol–gel reaction (Fig. 17).

After the immobilization of **27** *via* treatment with aminoethyltriethoxysolane in the presence of DCC and DMAP in THF, FSNT was characterized by SEM and TEM. The silica product exhibited a well-defined nanotube structure with a diameter of *ca.* 260 nm and several micrometres in length. The binding abilities of **27** for metal ions were assessed based on fluorescence changes occurring upon the addition of various cations—Li^+, Na^+, K^+, Cs^+, Mg^{2+}, Ca^{2+}, Ba^{2+}, Zn^{2+}, Ag^+, and Pb^{2+}—as perchlorates in water. Strong quenching of fluorescence of both monomer and excimer bands of the pyrene groups was observed only in the presence of Pb^{2+} (Fig. 18).

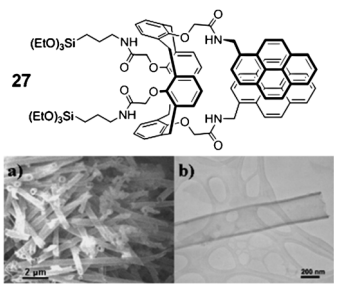

Fig. 17 (a) SEM and (b) TEM images of FSNT obtained from sol–gel reaction.

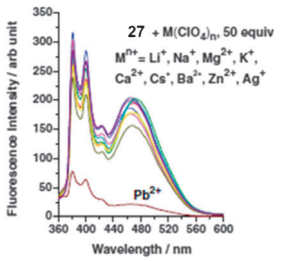

Fig. 18 Fluorescent spectra of FSNT upon the addition of cation perchlorate salts (50 equiv.) in water.

The stability constant of association of Pb^{2+} to **27** in water was calculated as 4.7×10^5 M^{-1}. The detection limitation of Pb^{2+} was 30 μm. The fluorescence behavior of **27** was attributed to a chelation of the Pb^{2+} by the two oxygen atoms of the amido functions, which resulted in a conformational change with a reduction in excimer emission.

Leray and Lebeau *et al.*[86] reported an ordered mesoporous silica functionalized by a covalently-bound calixarene-based fluorophore for the selective optical sensing of Hg^{2+} in water. Starting from the observation that cone calixarene **28** functionalized by two dansyl groups allows for the detection of Hg^{2+} in the 10^{-7} mol L^{-1} concentration range with a very high selectivity towards Hg^{2+} overpotential interfering cations (Na^+, K^+, Ca^{2+}, Cu^{2+}, Zn^{2+}, Cd^{2+}, and Pb^{2+}), they prepared analogue calixarene **29** possessing triethoxysilyl functionalities that will be used for grafting on silica. Long aliphatic chains were used to bear these functionalities in order not to disturb the ability of the calixarene moiety to complex Hg^{2+}.

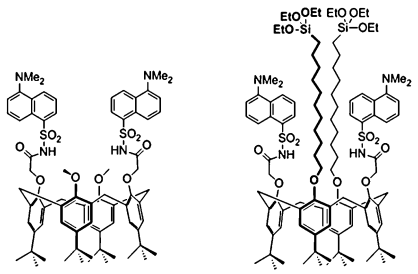

28 **29**

The grafting of calixarene **29** was achieved on known **SBA-15**[87] mesoporous silica by refluxing for 20 h in a suspension of silica in a toluene solution of **29**. The functionalized **29-SBA-15** product was characterized by XRD pattern and N_2-sorption, NMR spectroscopy, and TGA-DTA evidencing a hexagonal pattern similar to the starting silica material with the presence of organic moieties on the pore surfaces of mesoporous silica (Scheme 1).

The ability of **29-SBA-15** to detect Hg^{2+} in water was demonstrated by the observation of Hg^{2+} photophysical changes. A strong emission quenching of the emission spectra of **29-SBA-15** in the presence of increasing concentrations of Hg^{2+} was observed. This behavior was attributed to a deprotonation of the NH groups *via* complexation of the Hg^{2+} by the calixarene. A rapid response of few seconds was observed. The detection limit was 3.3×10^{-7} mol L^{-1}. Competing experiments demonstrated the very high Hg^{2+}-selectivity of **29-SBA-15** over interfering cations (Na^+, Cu^{2+}, and Pb^{2+}) at low concentration.

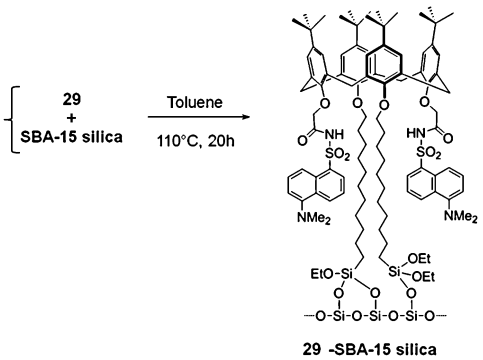

Scheme 1 Grafting of compound **29** on mesoporous silica particles.

Based on a previous work concerning the detection of host–guest interaction between a monolayer of dansyl on glass and β-cyclodextrin *via* fluorescence spectroscopy, Veggel and Reinhoudt *et al.*[88] reported a monolayer made of a Na^+-selective fluoroionophore on glass. Calix[4]arene (**30**) in cone conformation bearing at the lower rim four amido functions known to be Na^+-selective chelating sites[89,90] (over the other alkali metal cations) and two opposite pyrenyl groups as signal reporters were prepared to be grafted onto glass (Fig. 19).

The monolayers of Na^+-selective fluorescent **30** on glass were prepared *via* covalent coupling of the bis-isocyanate derivative of **30** to SAM of 3-aminopropyltriethoxysilane (APTES). Thus, the substrates functionalized with APTES SAM[91] were immersed in a solution of **30** and *N*,*N*-diisopropylethylamine in dichloromethane overnight. In the coupling reaction, the *p*-nitrophenyl carbamate groups are converted into isocyanates in the presence of a base which subsequently reacts with an amino-terminal surface to form urea bonds. The surface coverage was found to be 80% by ellipsometry and UV-vis absorption techniques. Fluorescence emission data of the monolayer upon the addition of sodium salt as an acetate in methanol resulted in an increase of the excimer while a reduction was observed for the monomer, showing that the complexation of sodium cation arranges the pyrene groups in a better position to form excimers than in the free ligand. Fitting the monomer fluorescence response yielded a binding constant of $K_{395\,nm} = 1540 \pm 700\ M^{-1}$. The fitting of the excimer fluorescence yielded $K_{475\,nm} = 5000 \pm 3000\ M^{-1}$. Similar experiments with potassium and caesium acetate failed to generate a significant response. Although no stability constants could be obtained, Na^+/K^+ and Na^+/Cs^+ selectivities were estimated to be larger than 100.

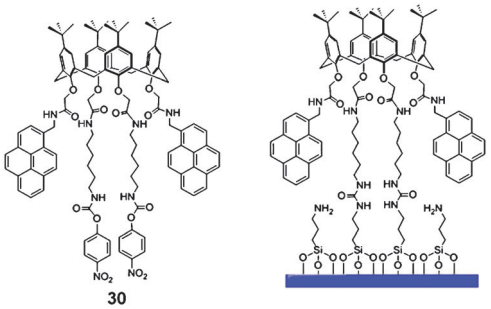

Fig. 19 Structure of fluoroionophore **30** (left) and schematic representation of the monolayer (right).

4.3. Organic molecule sensors

Timmerman and Yitzchaik *et al.*[92] have reported a tandem selective detector of neurotransmitter acetylcholine (ACh) composed of an analogue of **25** attached to the surface of an oxide-containing silicon surface. A previous study conducted by Lehn *et al.*[93] established that **25** and **26** are ACh-receptors with very high stability constants, the ACh being included in the aromatic cavity of the calixarene, as shown by the observed X-ray structures. Accordingly, Korbakov *et al.*[92] first studied the complex formation between **25**, **26**, and **32** and chromophore *trans*-4-4-(dimethylamino)styryl-1-methylpyridinium-*p*-toluene sulfonate (**D**) in water.

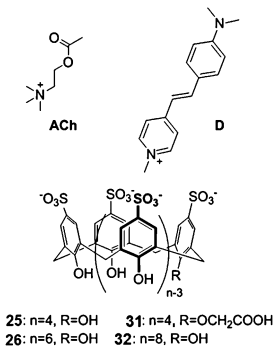

The formation of these complexes (**25**, **26**, or **32**) and **D** (with $K_a \approx 10^5\ M^{-1}$) was accompanied by a drastic increase (up to 20–60 fold) in the chromophore relative quantum yield and by a large hypsochromic shift of the emission band maximum of complexed **D**. Upon addition, ACh displaces chromophore **D** from the calixarene cavity as shown by the reappearance of the free chromophore emission band. It was demonstrated that (**25**, **26**, or **32**)-**D** complexes are capable of selectively sensing ACh in solution at sub-μM concentrations. The ACh detection limit was $\sim 5 \times 10^8$ M. Taking these results into account, the authors decided to immobilize **25-D** complex onto silica surfaces. For this purpose, water-soluble *O*-carbomethoxy-*p*-sulfonatocalix[4]arene (**31**), an analogue of **25**, was prepared and immobilized on an amino-terminated silicon surface by EDC coupling in the presence of NHS to facilitate the formation of amido bonds between the carboxylic acid of **31** and the amine at the silicon surface. The attachment of **31** was monitored by spectrometric ellipsometry and by advancing contact angle measurements. Ellipsometry spectrometry gave a layer thickness of *ca.* 9 ± 0.4 Å, consistent with the calculated value of 8–12 Å. **31**-Modified silicon samples were exposed to a solution of **D** in methanol to produce the desirable immobilized **25-D** complex onto silica. The emission band of the chromophore of **Si/25-D** was hypsochronically shifted to 584 nm from the band maximum at 604 nm for the free chromophore. Exposing **Si/25-D** to a solution of ACh induced a rapid decrease of the new emission band. As for the **D**-calix complexes, the optical behaviour was interpreted by a displacement of the chromophore **D** from the calix cavity *via* preferential complexation of ACh. Similar experiments conducted with solutions of neurotransmitters (tryptamine, glycine, aspartic acid, taurine, and noradrenaline) exhibited poor complexation ability. The removal of **D** from the

calixarene cavity by ACh is reminiscent of the results obtained by Katz and Iglesia *et al.*[81] for calixarenes grafted on silica; they determined that interactions of aromatic molecules with the calix cavity is stronger than the free calixarene in solution. The absence of solubilizing groups near the cavity increases the hydrophobic properties of the cavity.

5. Quantum dot-supported calixarenes

5.1. Principles

Of all available nanoparticles, semiconductor quantum dots (QDs) have been most extensively studied, owing to their novel optical, electrical, and catalytic properties, and have gained increasing attention during the past decade.[94] QDs have several important advantages, including size-selection, broad absorption, narrow emission bands, extreme brightness, and high photostability.[95] The principal advantage of the QD nanoparticles for the development of fluorescent sensors is that their luminescent emission depends on the size of the particle.[96] Many studies thus far conducted are focused on the development of new techniques for the synthesis of high-quality quantum dots with high-luminescence quantum yields and for the measurement of their photo-physical properties in analytical chemistry as high-sensitivity fluorescent sensors.[97] QDs can be readily capped with any organic ligand to modulate their complexing properties. They are very sensitive to surface interactions, due to the unique discrete electronic state of each particle. For instance, the control of optical properties of QDs by surface coating with calixarene carboxylic acids has been reported by Jin *et al.*[98,99] Here, the application of calixarene appended QDs as an organic ligand to the fluorescent chemosensing of various analytes was demonstrated.

5.2. Cation sensors

Compound **9**-capped QDs were prepared by mixing the S-Calix with a dilute solution of CdSe/ZnS in acetonitrile at room temperature by Li *et al.*[100] The AB pattern for the $ArCH_2Ar$ protons in the ^{1}H-NMR spectrum of **9** methylene protons suggested that **9** adopts a cone conformation. The fluorescence spectrum of **9** capped QDs is shown in Fig. 20. The quantum yield of **9** capped QDs is approximately 55%, which is far higher than that of thiol-modified CdSe/ZnS QDs. To examine the selectivity, the fluorescence titration of **9** capped QDs is conducted with a variety of metal ions. The **9** capped QDs evidence Hg^{2+} ion selectivity *via* a fluorescence intensity decrease, as receptor molecules with sulfur donor atoms preferred soft metal cations such as mercury ions. This quenching effect may be attributable to the effective electron transfer from **9** to Hg^{2+}. However, **9** capped QDs displays very weak response to the other metal ions (Li^+, Na^+, K^+, Mg^{2+}, Ca^{2+}, Cu^{2+}, Zn^{2+}, Mn^{2+}, Co^{2+}, and Ni^{2+}), even at a relatively higher concentration. The replacement of sulfur atoms by selenium to give Se-Calix, leading to Se-calix capped QDs with a quantum yield of approximately 45% at room temperature.[101]

Highly fluorescent water-soluble CdSe/ZnS (core/shell) QDs as a fluorescent Cu^{2+} ion probe were also synthesized by Jin *et al.*[102] using thiacalix[4]arene carboxylic acid **33** as a surface

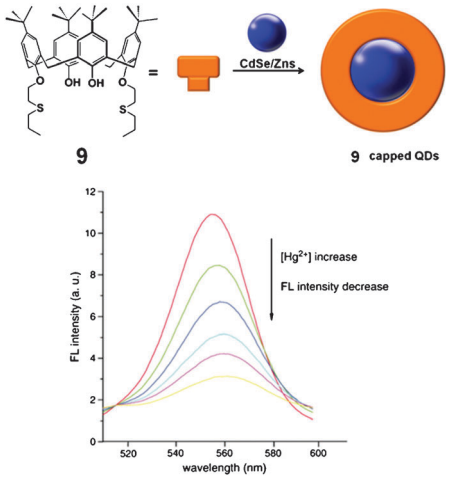

Fig. 20 Effect of Hg^{2+} concentration on FL intensity of **9** capped QDs.

coating agent. Hydrophobic trioctylphosphine oxide (TOPO)-capped CdSe/ZnS QDs were over-coated with the thiacalix[4]arene in THF at room temperature, and the deprotonation of the carboxylic acids resulted in the formation of water-soluble QDs. The surface structures of the QDs were characterized *via* TEM and fluorescence correlation spectroscopy (FCS). The TEM images demonstrated that **33**-coated QDs were monodispersed with a particle size (core-shell moiety) of approximately 5 nm. The hydrodynamic diameter of the QDs was determined to be 8.9 nm by FCS, demonstrating that the thickness of the surface organic layer of the QDs was approximately 2 nm. These results show that the surface layer forms a bilayer structure consisting of TOPO and thiacalix[4]arene molecules. **33**-coated CdSe/ZnS QDs were highly fluorescent (quantum yield, 0.21) compared to the QDs surface-modified with mercaptoacetic acid and mercaptoundecanoic acid. The fluorescence of the **33**-coated QDs was effectively quenched by Cu^{2+} ions even in the presence of other transition metal ions such as Cd^{2+}, Zn^{2+}, Co^{2+}, Fe^{2+}, and Fe^{3+} ions in the same solution. The Stern–Volmer plot for

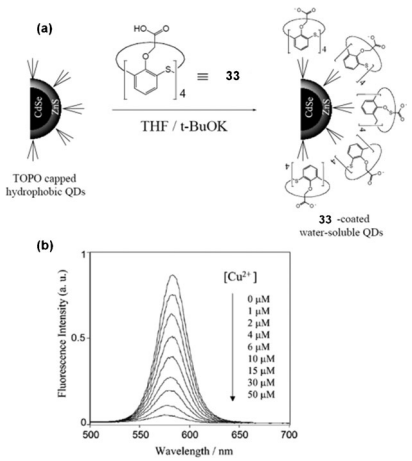

Fig. 21 (a) Surface modification of TOPO-capped CdSe/ZnS QDs with **33** in THF. (b) Effect of Cu^{2+} ions on the fluorescence spectra of **33**-coated QDs in an aqueous solution (pH 9.2). The absorbance at an excitation wavelength of 480 nm was adjusted to be 0.05 for the QDs.

the fluorescence quenching by Cu^{2+} ions exhibited a linear relationship up to 30 μM of Cu^{2+} ions. The ion selectivity of **33**-coated QDs was determined *via* measurements of fluorescence responses toward biologically important transition metal ions (50 μM) including Fe^{2+}, Fe^{3+}, Co^{2+} > Zn^{2+}, Cd^{2+}. The fluorescence of **33**-coated QDs was almost insensitive to other biologically important ions such as Na^{+}, K^{+}, Mg^{2+}, and Ca^{2+}, suggesting that thiacalix[4]arene-coated QDs can be employed as a fluorescent Cu^{2+} ion probe for biological samples (Fig. 21).

5.3. Biomolecule sensors

Jin *et al.*[103] have presented water-soluble CdSe/ZnS QDs surface-modified with amphiphilic *p*-sulfonatocalix[4]arene (**35**) for the optical detection of the neurotransmitter ACh. The QDs evidenced very weak emission, when **25** and **34** were used as the surface-coating agents, and they were decomposed after several hours in water. However, in the case of **35**, highly fluorescent and stable, water-soluble QDs were obtained. The higher emission efficiency observed for **35**-coated QDs is in comparison with MAA(mercaptoacetic acid)-coated QDs. It may be explained by a higher barrier toward the access of water molecules to the QD surface. The **35**-coated QDs evidence significantly quenched fluorescence when ACh was added. An approximate 50% fluorescence quenching was noted in the presence of 1×10^{-3} M of ACh. The emission quenching of the **35**-coated QDs is quite selective to ACh over other neurotransmitter compounds. It should be noted that the addition of ACh does not alter the spectral widths and the emission maximum of the QDs without amphiphilic *p*-sulfonatocalix[4]arene (**25**). This result indicates that ACh does not induce surface deterioration or aggregation in the **35**-coated QDs (Fig. 22).

A similar system was reported by Li *et al.*[104] A simple, rapid ligand exchange route for the preparation of highly fluorescent, stable and water-soluble CdSe QDs was obtained using **25** and **26** rather than the original TOPO ligands (Fig. 23).

The ligands were found to exert a profound effect on the luminescence response of QDs to amino acids. The **25**-coated CdSe QDs were sensitive to methionine. On the other hand, **26**-coated CdSe QDs turned out to be sensitive to

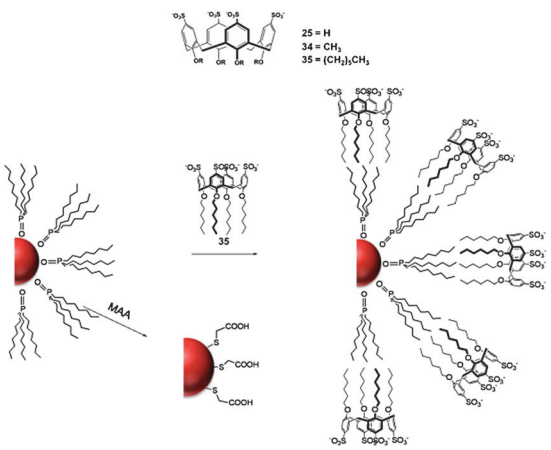

Fig. 22 A schematic representation of the surface-coating of TOPO capped CdSe/ZnS QDs with **35** and MAA.

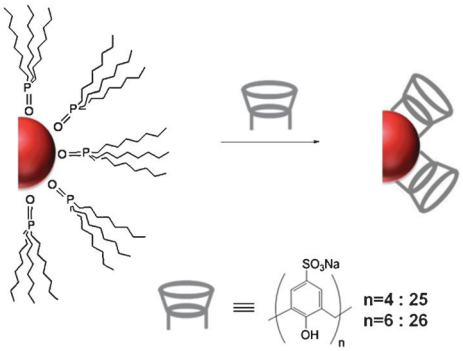

Fig. 23 A schematic representation of the synthesis of the **25** and **26** coated CdSe QDs by ligand exchange.

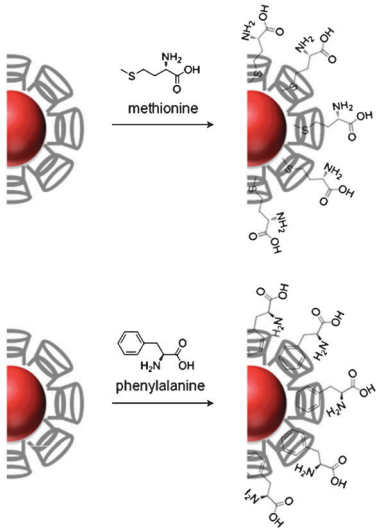

Fig. 24 A schematic illustration of the possible mechanisms of methionine and phenylalanine enhancing the fluorescence of **25** and **26** coated CdSe QDs.

phenylalanine. To demonstrate the detection capability of these new probes, **25**- and **26**-coated CdSe QDs were employed to detect methionine and phenylalanine in physiological buffer solution. Under optimal conditions, the relative fluorescence intensities of the **25**- and **26**-coated QDs increased in a linear fashion with increasing concentrations of amino acids. Methionine and phenylalanine enhanced the luminescence of **25**- and **26**-coated QDs with a concentration dependence that was best described by a Langmuir-type equation. The enhancement of luminescence was proposed to be attributable to a complexation of amino acids in the cavity of **25** and **26** (Fig. 24).

5.4. Quantum dots-SiO_2-supported-calixarenes

Li *et al.*[105] reported on the highly luminescent and stable calixarene **36**- and **37**-coated silica nanospheres englobed with CdTe nanocrystals. They were prepared *via* a sol–gel technique in aqueous media, and were characterized by luminescence spectroscopy, UV-vis, FT-IR spectroscopy, TEM, *etc*. The nanocomposites (**36** or **37**@SiO_2@CdTe) evidenced strong fluorescence and were more stable than the SiO_2@CdTe NPs. The **36** or **37**@SiO_2@CdTe NPs allowed for highly

sensitive determinations of PAHs *via* enhancement of the fluorescence intensity response. The **36**@SiO_2@CdTe NPs turned out to be sensitive to the presence of anthracene, and the relative fluorescence intensities of **36**@SiO_2@CdTe increased in a linear fashion with increasing anthracene concentration in the range 0.1–50 mM, with the corresponding detection limits (3α) of 2.45×10^{-8} M. Interestingly, the **37**@SiO_2@CdTe NPs turned out to be sensitive to the presence of pyrene. Under optimal conditions, the relative fluorescence intensities of **37**@SiO_2@CdTe NPs both increased linearly with increasing pyrene concentration in the range 0.1–50 mM, with corresponding detection limits (3α) of 2.94×10^{-8} M. However, the fluorescence response of **36** or **37**@SiO_2@CdTe NPs to other PAHs (including acenaphthene, anthracene, 9,9-difluorofluorene, carbazole, fluoranthene, phenanthrene, biphenyl, fluorene, pyrene) proved to be negligible. It was reasonable to believe that **36** or **37**@SiO_2@CdTe nanocomposites played an important role in the recognition of different size PAHs, due to the fact that **36** or **37**@SiO_2@CdTe contains a π-wall cavity that may readily complex with aromatic compounds through π–π interactions, hydrophobic interactions, host–guest interactions, *etc*. (Fig. 25).

Mann *et al.*[106] reported on the nanoscaled organization of CdS QDs on structurally persistent dendro-calixarene micelles. UV-vis spectra of CdS-dendrocalixarene micelles evidenced a broad adsorption band for the calixarene at 270 nm and an absorption edge associated with the CdS NPs. The sequestration of pyrene within the hydrophobic interior was demonstrated by optical emission, which showed high-intensity peaks at 394 and 630 nm corresponding to the fluorescence (singlet) and the phosphorescence (triplet) emission.

Li and Qu[107] synthesized CdTe QDs nanocrystals in sol–gel-derived composite silica spheres coated with calix[4]arene and their applications as fluorescent probes for the detection of pesticides. CdTe QDs nanocrystals in sol–gel-derived composite silica spheres were prepared from CdTe QDs *via* the Stöber method.[108] SiO_2@CdTe NPs were coated with **36** as shown in Fig. 26.

36@SiO_2@CdTe NPs were characterized by fluorescence and IR spectrometries. TEM images and PCS measurements showed the average sizes of SiO_2@CdTe NPs and **36**@SiO_2@CdTe NPs were approximately 70 and 100 nm, respectively. Fluorescence titrations (512 nm) of SiO_2@CdTe NPs and **36**@SiO_2@CdTe NPs were conducted in water at

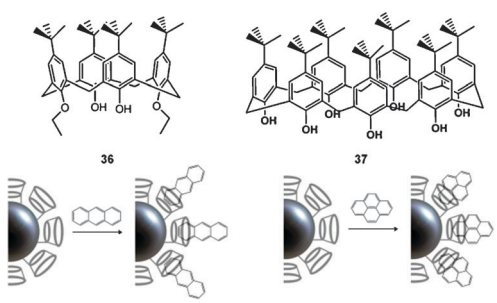

Fig. 25 Schematic illustration of possible structures of **36**@SiO_2@CdTe NPs-anthracene and **37**@SiO_2@CdTe NPs-pyrene.

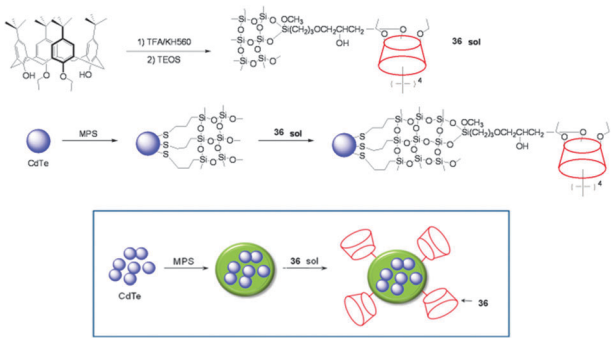

Fig. 26 Formation of **36**@SiO_2@CdTe NPs.

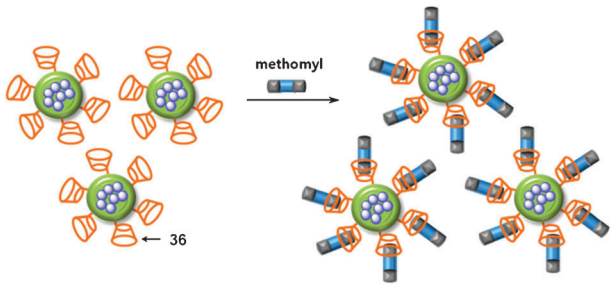

Fig. 27 Schematic illustration of a possible structure of the **36**@SiO_2@CdTe NPs-methomyl.

pH = 8.0 with various pesticides (parathion-methyl, methomyl, optunal, fenamilthion, and acetamprid) to evaluate their selectivity of complexation. Methomyl was shown to be the pesticide providing the most substantial increase in fluorescent intensity. This was attributed to the fact that the cavity of **36** was not sufficiently large to accommodate aromatic pesticides, as well as its preference for the linear methomyl. A detailed study conducted with methomyl indicated a complexation mechanism involving the filling of the calix cavity by methomyl with a conformational rigidification of the surface substituents suppressing the quenching pass to the medium by effective cone protection, giving rise to an increase in the fluorescent intensity, as illustrated in Fig. 27.

6. Conclusions

The development of novel methods in chemical and biological fields that permit the real-time detection of different compounds with high accuracy, precision, reproducibility, and low molecular detection limits is a profound challenge. This is possible, in particular, by virtue of the combination of the optical properties of nanostructured metals and the advanced chemical properties of self-assembled calixarenes. On the basis of the concepts and principles of supramolecular chemistry, and particularly molecular recognition and self-assembly and the chemistry of hybrid inorganic–organic materials and nanomaterials, we have collected in this review the nanoscaled construction and application of luminescent nanoparticles based on calixarenes and different surfaces: gold, silica, silver, and quantum dots. Moreover, the host–guest interaction mechanism leading to the formation of a complex between functionalized nanoparticles and different substrates has been highlighted.

Several perspectives can be drawn in regard to the development of optical host–guest systems of calixarenes on the surfaces of nanoparticles. For instance, catalytic systems have been described based on calixarenes grafted on titanium oxide and titanium–silica surfaces, which may be transformed into optical nanoparticles. Chiral surface plasmon resonance has been previously described by the postsynthetic modification of gold particles with calixarene enantiomers, which may lead to the optical recognition of a chiral object.

More generally, plasmons in strongly coupled metallic nanostructures may be used to enlarge the panels of this type of optical system. New mineral solid surfaces have been reported which may be used as new supports, such as mesoporous non-oxide materials. In another field, hybrid materials could be prepared from polymers presenting channeled structures that may prove useful in the formation of organized molecular surfaces.

Acknowledgements

This work was supported by a grant from the CRI program (2011-0000420) to J. S. Kim.

Notes and references

1 J. C. Love, L. A. Estroff, J. K. Kriebel, R. G. Nuzzo and G. M. Whitesides, *Chem. Rev.*, 2005, **105**, 1103–1170.
2 D. M. Vriezema, M. C. Aragonès, J. A. A. W. Elemans, J. J. L. M. Cornelissen, A. E. Rowan and R. J. M. Nolte, *Chem. Rev.*, 2005, **105**, 1445–1489.
3 J. J. Gooding and S. Ciampi, *Chem. Soc. Rev.*, 2011, **40**, 2704–2718.
4 U. Drechsler, B. Erdogan and V. M. Rotello, *Chem.–Eur. J.*, 2004, **10**, 5570–5579.
5 Themed issue on Functional Nanostructures, *Chem. Rev.*, 2005, **105**, issue 4.
6 Themed issue on Hybrid materials, *Chem. Soc. Rev.*, 2011, **40**, issue 1.
7 C. Sanchez, K. J. Shea and S. Kitagawa, *Chem. Soc. Rev.*, 2011, **40**, 471–472.
8 C. D. Gutsche, *Calixarenes Revisited*, The Royal Society of Chemistry, Cambridge, 1998.
9 J. Vicens and V. Böhmer, in *Calixarenes: A Versatile Class of Macrocyclic Compounds*, ed. J. E. D. Davies, Kluwer Academic Publishers, Dordrecht, Holland, 1991.
10 *Calixarenes 2001*, ed. Z. Asfari, V. Böhmer, J. Harrowfield and J. Vicens, Kluwer Academic Publishers, Dordrecht, Holland, 2001.
11 *Calixarenes for Separations*, ACS Symposium series 757, ed. G. L. Luminetta, R. D. Rogers and A. S. Gopolan, American Chemical Society, Washington, US, 2000.
12 *Calixarenes in Action*, ed. L. Mandolini and R. Ungaro, Imperial College Press, London, UK, 2000.
13 *Calixarenes in the Nanoworld*, ed. J. Vicens and J. Harrowfield, Springer, Dordrecht, Holland, 2007.
14 A. Wei, *Chem. Commun.*, 2006, 1581–1591.
15 K. Heltunen and P. Shahgadian, *New J. Chem.*, 2010, **34**, 2704–2714.
16 A. I. Konovalov and I. S. Antipin, *Mendeleev Commun.*, 2008, **18**, 229–237.
17 B. Mokhtari, K. Pourabdollah and N. Dalali, *J. Inclusion Phenom. Macrocyclic Chem.*, 2011, **69**, 1–55.
18 B. Mokhtari, K. Pourabdollah and N. Dalali, *J. Radioanal. Nucl. Chem.*, 2011, **287**, 921–934.
19 S. Sameni, C. Jeunesse, D. Matt and J. Harrowfield, *Chem. Soc. Rev.*, 2009, **38**, 2117–2146.
20 L. Mutihac, J. H. Lee, J. S. Kim and J. Vicens, *Chem. Soc. Rev.*, 2011, **40**, 2777–2796.
21 A. Dondoni and A. Marra, *Chem. Rev.*, 2010, **110**, 4949–4977.
22 I. Leray and B. Valeur, *Eur. J. Inorg. Chem.*, 2009, 3525–3535.
23 J. S. Kim, S. Y. Lee, J. Yoon and J. Vicens, *Chem. Commun.*, 2009, 4791–4802.
24 Y.-S. Zhang and J. Luo, *J. Inclusion Phenom. Macrocyclic Chem.*, 2011, DOI: 10.1007/s10847-011-9935-4.
25 (*a*) M. C. Daniel and D. Astruc, *Chem. Rev.*, 2004, **104**, 293–346; (*b*) A. C. Templeton, M. P. Wuelfing and R. W. Murray, *Acc. Chem. Res.*, 2000, **33**, 27–36.
26 C. Vericat, M. E. Vela, G. Benitez, P. Carro and R. C. Salvarezza, *Chem. Soc. Rev.*, 2010, **39**, 1805–1834.
27 S. Link and M. A. El-Sayed, *Int. Rev. Phys. Chem.*, 2000, **19**, 409–453.
28 P. V. Kamat, *J. Phys. Chem. B*, 2002, **106**, 7729–7744.
29 K. Kneipp, H. Kneipp, I. Itzkan, R. R. Dasari and M. S. Feld, *Chem. Rev.*, 1999, **99**, 2957–2975.
30 (*a*) G. Schmid, *Clusters and Colloids: From Theory to Applications*, VCH, New York, 1994; (*b*) A. Henglein, *J. Phys. Chem.*, 1993, **97**, 5457–5471; (*c*) U. Kreibig and L. Genzel, *Surf. Sci.*, 1985, **156**, 678–700; (*d*) L. S. Marie and A. F. Colby Jr., *J. Phys. Chem. B*, 1999, **103**, 11398–11406; (*e*) D. G. Christian, M. S. Adam, J. N. Thaddeus Jr. and Z. Z. Jin, *J. Am. Chem. Soc.*, 2003, **125**, 549–553; (*f*) Y. Takeuchi, T. Ida and K. Kimura, *Surf. Rev. Lett.*, 1996, **3**, 1205–1208; (*g*) K. L. Kelly, E. Coronado, L. L. Zhao and G. C. Schatz, *J. Phys. Chem. B*, 2003, **107**, 668–677; (*h*) S. Link, M. B. Mohamed and M. A. El-Sayed, *J. Phys. Chem. B*, 1999, **103**, 3073–3077; (*i*) Z. Zhong, S. Patskovskyy, P. Bouvrette, J. H. T. Luong and A. Gedanken, *J. Phys. Chem. B*, 2004, **108**, 4046–4052; (*j*) S. Link and M. A. El-Sayed, *J. Phys. Chem. B*, 1999, **103**, 8410–8426; (*k*) P. Mulvaney, *Langmuir*, 1996, **12**, 788–800.
31 (*a*) Y. Kim, R. C. Johnson and J. T. Hupp, *Nano Lett.*, 2001, **1**, 165–167; (*b*) T. B. Norsten, B. L. Frankamp and V. M. Rotello, *Nano Lett.*, 2002, **2**, 1345–1348; (*c*) S. O. Obare, R. E. Hollowell and C. J. Murphy, *Langmuir*, 2002, **18**, 10407–10410; (*d*) S.-Y. Lin, S.-W. Liu, C.-M. Lin and C.-H. Chen, *Anal. Chem.*, 2002, **74**, 330–335; (*e*) A. Sugunan, C. Thanachayanont, J. Dutta and J. G. Hilborn, *Sci. Technol. Adv. Mater.*, 2005, **6**, 335–340; (*f*) C. A. Mirkin, R. L. Letsinger, R. C. Mucic and J. J. Storhoff, *Nature*, 1996, **382**, 607–609; (*g*) R. Elghanian, J. J. Storhoff, R. C. Mucic, R. L. Letsinger and C. A. Mirkin, *Science*, 1997, **277**, 1078–1081; (*h*) R. A. Reynolds III., C. A. Mirkin and R. L. Letsinger, *J. Am. Chem. Soc.*, 2000, **122**, 3795–3796; (*i*) K. Sato, M. Onoguchi, Y. Sato, K. Hosokawa and M. Maeda, *Anal. Biochem.*, 2006, **350**, 162–164; (*j*) K. Sato, K. Hosokawa and M. Maeda, *J. Am. Chem. Soc.*, 2003, **125**, 8012–8103; (*k*) J. J. Storhoff, R. Elghanian, R. C. Mucic, C. A. Mirkin and R. L. Letsinger, *J. Am. Chem. Soc.*, 1998, **120**, 1959–1964; (*l*) J. J. Storhoff, A. A. Lazarides, R. C. Mucic, C. A. Mirkin, R. L. Letsinger and G. C. Schatz, *J. Am. Chem. Soc.*, 2000, **122**, 4640–4650; (*m*) S.-J. Park, A. A. Lazarides, C. A. Mirkin and R. L. Letsinger, *Angew. Chem., Int. Ed.*, 2001, **40**, 2909–2912; (*n*) J.-M. Nam, S.-J. Park and C. A. Mirkin, *J. Am. Chem. Soc.*, 2002, **124**, 3820–3821; (*o*) S. Cobbe, S. Connolly, D. Ryan, L. Nagle, R. Eritja and D. Fitzmaurice, *J. Phys. Chem. B*, 2003, **107**, 470–477; (*p*) P. J. Costanzo, T. E. Patten and T. A. P. Seery, *Chem. Mater.*, 2004, **16**, 1775–1785; (*q*) H. Otsuka, Y. Akiyama, Y. Nagasaki and K. Kataoka, *J. Am. Chem. Soc.*, 2001, **123**, 8226–8230; (*r*) C.-C. Huang, Y.-F. Huang, Z. Cao, W. Tan and H.-T. Chang, *Anal. Chem.*, 2005, **77**, 5735–5741; (*s*) H. Yao, K. Miki, N. Nishida, A. Sasaki and K. Kimura, *J. Am. Chem. Soc.*, 2005, **127**, 15536–15543.
32 H. Chen, Y.-S. Gal, S.-H. Kim, H.-J. Choi, M.-C. Oh, J. Lee and K. Koh, *Sens. Actuators, B*, 2008, **133**, 577–581.
33 M. J. Esplandiu and H. Hagenstrom, *Solid State Ionics*, 2002, **150**, 39–52.
34 H. Schoenherr, G. J. Vancso, B. H. Huisman, F. C. J. M. Veggel and D. N. Reinhoudt, *Langmuir*, 1999, **15**, 5541–5546.
35 K. Tamada, J. Nagasawa, F. Nakanishi, K. Abe, M. Hara, W. Knoll, T. Ishida, H. Fukushima, S. Miyashita, T. Usui, T. Koini and T. R. Lee, *Thin Solid Films*, 1998, **327**, 150–155.
36 H.-F. Ji, E. Finot, R. Dabestani, T. Thundat, G. M. Brown and P. F. Britt, *Chem. Commun.*, 2000, 457–458.
37 S. Zhang and L. Echegoyen, *Tetrahedron Lett.*, 2003, **44**, 9079–9082.

38 Z. Asfari, R. Abidi, F. Amaud and J. Vicens, *J. Inclusion Phenom. Macrocyclic Chem.*, 1992, **13**, 163–169.
39 S. Zhang, F. Song and L. Echegoyen, *Eur. J. Org. Chem.*, 2004, 2936–2943.
40 Z. Wang, Q. Y. Zheng and Y. Chen, *Anal. Lett.*, 2001, **34**, 2609–2619.
41 H. Yan, J. Luo, H.-M. Xie, D.-X. Xie, Q. Su, J. Yin, B. N. Wanjala, H. Diao, D.-L. An and C.-J. Zhong, *Phys. Chem. Chem. Phys.*, 2011, **13**, 5824–5830.
42 S. Zhang, A. Palkar and L. Echegoyen, *Langmuir*, 2006, **22**, 10732–10738.
43 S. Zhang and L. Echegoyen, *Org. Lett.*, 2004, **6**, 791–794.
44 G. Patel and S. Menon, *Chem. Commun.*, 2009, 3563–3565.
45 K. Nakano, S. Tanaka, M. Takagi and S. Shinkai, *Bunseki Kagaku*, 2002, **51**, 409–413.
46 A. Friggeri, F. C. J. M. vanVeggel and D. N. Reinhoudt, *Chem.–Eur. J.*, 1999, **5**, 3595–3602.
47 H. Chen, M. Lee, S. Choi, J.-H. Kim, H.-J. Choi, S.-H. Kim, J. Lee and K. Koh, *Sensors*, 2007, **7**, 1091–1107.
48 H. Chen, Y. S. Kim, J. Lee, S. J. Yoon, D. S. Lim, H.-J. Choi and K. Koh, *Sensors*, 2007, **7**, 2263–2272.
49 C. Han, L. Zeng, H. Li and G. Xie, *Sens. Actuators, B*, 2009, **137**, 704–709.
50 A. Arduini, D. Demuru, A. Pochini and A. Secchi, *Chem. Commun.*, 2005, 645–647.
51 S. Zhang and L. Echegoyen, *J. Org. Chem.*, 2005, **70**, 9874–9881.
52 G. M. Whitesides, J. P. Mathias and C. T. Seto, *Science*, 1991, **254**, 1312–1319.
53 G. M. Whitesides, *Small*, 2005, **1**, 172–179.
54 V. Balzani, *Small*, 2005, **1**, 278–283.
55 R. Shenhar and V. M. Rotello, *Acc. Chem. Res.*, 2003, **36**, 549–561.
56 K. K. Y. Wong and X. Liu, *Med. Chem. Commun.*, 2010, **1**, 125–131.
57 L. S. Nair and C. T. Laurencin, *J. Biomed. Nanotechnol.*, 2007, **3**, 301–316.
58 H. M. Rowe, S. P. Chan, J. N. Demas and B. A. DeGraff, *Anal. Chem.*, 2002, **74**, 4821–4827.
59 J. Liu, J. Alvarez, W. Ong and A. E. Kaifer, *Nano Lett.*, 2001, **1**, 57–60.
60 X. Lu and E. Masson, *Langmuir*, 2011, **27**, 3051–3058.
61 J. D. Gibson, B. P. Khanal and E. R. Zubarev, *J. Am. Chem. Soc.*, 2007, **129**, 11653–11661.
62 R.-C. Mutihac and H. Riegler, *Langmuir*, 2010, **26**, 6394–6399.
63 N. Leopold and B. Lendl, *J. Phys. Chem. B*, 2003, **107**, 5723–5727.
64 M. V. Canamares, J. V. Garcia-Ramos, J. D. Gomez-Varga, C. Domingo and S. Sanchez-Cortes, *Langmuir*, 2005, **21**, 8546–8553.
65 J. Liu, W. Ong, A. E. Kaifer and C. Peinador, *Langmuir*, 2002, **18**, 5981–5983.
66 Y. Brian, C. Li and H. Li, *Talanta*, 2010, **81**, 1028–1033.
67 R. G. Harvey, *Polycyclic Aromatic Hydrocarbons*, J. Wiley & Sons, New York, 1997.
68 P. Leyton, S. Sanchez-Cortes, J. V. Garcia-Ramos, C. Domingo, M. Campos-Vallette, C. Saitz and R. E. Clavijo, *J. Phys. Chem. B*, 2004, **108**, 17484–17490.
69 P. Leyton, S. Sanchez-Cortes, M. Campos-Vallette, C. Domingo, J. V. Garcia-Ramos and C. Saitz, *Appl. Spectrosc.*, 2005, **59**, 1009–1015.
70 G. D. Thorn and R. A. Ludwig, *The Dithiocarbamates and Relates Compounds*, Elsevier Publishing Company, Amsterdam, 1962.
71 L. Guerrini, J. V. Garcia-Ramos, C. Domingo and S. Sanchez-Cortes, *Langmuir*, 2006, **22**, 10924–10926.
72 L. Guerrini, J. V. Garcia-Ramos, C. Domingo and S. Sanchez-Cortes, *Anal. Chem.*, 2009, **81**, 953–960.
73 S. Sanchez-Cortes, C. Domingo, J. V. Garcia-Ramos and J. A. Aznarez, *Langmuir*, 2001, **17**, 1157–1162.
74 D. Xiong and H. Li, *Nanotechnology*, 2008, **19**, 465502–465507.
75 L. Shang, Y. L. Wang, L. J. Huang and S. J. Dong, *Langmuir*, 2007, **23**, 7738–7744.
76 Q. Xiao, B. Hu, C. H. Yu, L. B. Xia and Z. C. Jiang, *Talanta*, 2006, **69**, 848–855.
77 D. Xiong, M. Chen and H. Li, *Chem. Commun.*, 2008, 880–882.
78 F. Hoffmann and M. Fröba, *Chem. Soc. Rev.*, 2011, **40**, 608–620.
79 W. S. Han, H. Y. Lee, S. H. Jung, S. J. Lee and J. H. Jung, *Chem. Soc. Rev.*, 2009, **38**, 1904–1915.
80 A. Katz, P. Da Costa, A. C. P. Lam and J. M. Notenstein, *Chem. Mater.*, 2002, **14**, 3364–3368.
81 J. M. Notenstein, A. Katz and E. Iglesia, *Langmuir*, 2006, **22**, 4004–4014.
82 Q. Liang, B. Guan and M. Jiang, *J. Mater. Chem.*, 2010, **20**, 8236–8239.
83 T.-H. Tran-Thi, R. Dagnelie, S. Crunaire and L. Nicole, *Chem. Soc. Rev.*, 2011, **40**, 621–639.
84 J. H. Jung, M. Park and S. Shinkai, *Chem. Soc. Rev.*, 2010, **39**, 4286–4302.
85 T. H. Kim, J. H. Jung, J. K. Choi, Y. H. Choi, S. J. Lee, M. L. Seo and J. S. Kim, *Chem. Lett.*, 2007, **36**, 360–361.
86 R. Métivier, I. Leray, B. Lebeau and B. Valeur, *J. Mater. Chem.*, 2005, **15**, 2965–2973.
87 D. Zhao, J. Feng, Q. Huo, N. Melosh, G. H. Fredrickson, B. F. Chemla and G. D. Stucky, *Science*, 1998, **279**, 548–552.
88 N. J. van der Veen, S. Flink, M. A. Deij, R. J. M. Egberink, F. C. J. M. van Veggel and D. N. Reinhoudt, *J. Am. Chem. Soc.*, 2000, **122**, 6112–6113.
89 A. Arduini, E. Ghidini, A. Pochini, R. Ungaro, G. D. Andreetti, G. Castellani and F. Ugozolli, *J. Inclusion Phenom.*, 1988, **6**, 119–134.
90 J. A. J. Brunink, J. G. Bomer, W. Verboom, J. F. J. Engbersen and D. N. Reinhoudt, *Sens. Actuators, B*, 1993, **15**, 195–198.
91 D. G. Kurth and T. Bein, *Langmuir*, 1993, **9**, 2965–2973.
92 N. Korbakov, P. Timmerman, N. Lidich, B. Urbach, A. Sáar and S. Yitzchaik, *Langmuir*, 2008, **24**, 2580–2587.
93 J.-M. Lehn, R. Meri, J.-P. Vigneron, M. Cesario, J. Guilhem, C. Pascard, Z. Asfari and J. Vicens, *Supramol. Chem.*, 1995, **5**, 97–103.
94 M. Nirmal and L. Brus, *Acc. Chem. Res.*, 1999, **32**, 407–414.
95 W. C. W. Chan, D. J. Maxwell, X. Gao, R. E. Bailey, M. Han and S. Nie, *Curr. Opin. Biotechnol.*, 2002, **13**, 40–46.
96 M. J. Bruchez, M. Moronne, P. Gin, S. Weiss and A. P. Alivisatos, *Science*, 1998, **281**, 2013–2016.
97 Y. F. Chen and Z. Rosenzweig, *Anal. Chem.*, 2002, **74**, 5132–5138.
98 T. Jin, F. Fujii, E. Yamada, Y. Nodasaka and M. Kinjo, *J. Am. Chem. Soc.*, 2006, **128**, 9288–9289.
99 T. Jin, F. Fujii, H. Sakata, M. Tamura and M. Kinjo, *Chem. Commun.*, 2005, 2829–2831.
100 H. Li, Y. Zhang, X. Wang, D. Xiong and Y. Bai, *Mater. Lett.*, 2007, **61**, 1474–1477.
101 H. Li, W. Xiong, Y. Yan, J. Liu, H. Xu and X. Yang, *Mater. Lett.*, 2006, **60**, 703–705.
102 T. Jin, F. Fujii, E. Yamada, Y. Nodasaka and M. Kinjo, *Comb. Chem. High Throughput Screening*, 2007, **10**, 473–479.
103 T. Jin, F. Fujii, H. Sakata, M. Tamura and M. Kinjo, *Chem. Commun.*, 2005, 4300–4302.
104 X. Wang, J. Wu, F. Li and H. Li, *Nanotechnology*, 2008, **19**, 205501–205510.
105 H. Li and F. Qu, *J. Mater. Chem.*, 2007, **17**, 3536–3544.
106 K. K. Perkin, K. M. Bromley, S. A. Davis, A. Hirsch, C. Böttcher and S. Mann, *Small*, 2007, **3**, 2057–2060.
107 H. Li and F. Qu, *Chem. Mater.*, 2007, **19**, 4148–4154.
108 (*a*) M. Y. Gao, S. Kirstein, H. Mohwald, A. L. Rogach, A. Kornowski, A. Eychmuller and H. Weller, *J. Phys. Chem. B*, 1998, **102**, 8360–8363; (*b*) W. Stöber, A. Fink and E. Bohn, *J. Colloid Interface Sci.*, 1968, **26**, 62–69.

